Final Report
(Electron Beam Pumped Laser Action in Selenium and Tellurium with Applications for Tunable Backward Parametric Oscillations)

The Ohio State University

ElectroScience Laboratory

Department of Electrical Engineering
Columbus, Ohio 43212

Final Report 2679-4

September 1970

Grant Number NGR 36-008-103

National Aeronautics and Space Administration
Office of Grants and Research Contracts
Washington, D.C. 20546

NOTICES

When Government drawings, specifications, or other data are used for any purpose other than in connection with a definitely related Government procurement operation, the United States Government thereby incurs no responsibility nor any obligation whatsoever, and the fact that the Government may have formulated, furnished, or in any way supplied the said drawings, specifications, or other data, is not to be regarded by implication or otherwise as in any manner licensing the holder or any other person or corporation, or conveying any rights or permission to manufacture, use, or sell any patented invention that may in any way be related thereto.

REPORT
by
THE OHIO STATE UNIVERSITY ELECTROSCIENCE LABORATORY
Columbus, Ohio 43212

Sponsor	National Aeronautics and Space Administration Office of Grants and Research Contracts Washington, D.C. 20546
Grant Number	NGR 36-008-103
Investigation of	Electron Beam Pumped Laser Action in Selenium and Tellurium with Applications for Tunable Backward Parametric Oscillations
Subject of Report	Final Report
Submitted by	ElectroScience Laboratory Department of Electrical Engineering The Ohio State University
Date	September 1970

CONTENTS

ABSTRACT

Attempts to grow good quality single crystals of various alloy compositions Se_xTe_{1-x} with $0 \leq x \leq .5$ using a modified Bridgman have been only moderately successful. However, a pure Se (i.e., x = 0) crystal with an optical absorption constant $\alpha < 2$ cm^{-1} has been grown.

Photoconductivity studies indicate existence of a defect level below the band edge which varied smoothly with alloy composition. Width of the photoconductivity spectral response in the alloy crystals indicated that the crystals were of poorer quality than the pure Se crystals.

Thermally stimulated current measurements showed a plethora of deep defect levels in all crystals. Cathodoluminescence experiments were difficult to carry out; but weak red emission was observed on two occasions.

I. INTRODUCTION

This project was concerned with the growth and characterization of Se and Se_xTe_{1-x} alloy crystals for use in devices requiring certain optical characteristics. The peculiar spiral chain structure of trigonal Se and Te make these materials of special interest in the investigation of nonlinear optical phenomena. Also, the continuous range of alloy crystals can be grown, giving a continual gradation in properties such as bandgap, nonlinear susceptibility, birefringence, and photoconductance in going from pure Se to pure Te.

The first problem to be considered is the growth of good quality single crystals. A modified Bridgman technique is currently being used. This has produced crystals of various alloy compositions Se_xTe_{1-x} with x in the range of $0 \leq x \leq .5$. The quality of the alloy crystals has not been remarkable. However, a pure Se (i.e., $x = 0$) crystal with an optical absorption constant $\alpha < 2\ cm^{-1}$ has been grown.

In an attempt to identify some of the crystal defects which might be responsible for the residual optical absorption, various photoelectronic effects were investigated. Photoconductivity data showed the existence of a defect level below the band edge which varied smoothly with alloy composition. Width of the photoconductivity spectral response was larger in the alloy crystals than in the pure Se crystals, indicating the poorer quality of these crystals.

Thermally stimulated current measurements showed a plethora of deep defect levels, especially in the alloy crystals.

Cathodoluminescence experiments were plagued with difficulties. However, weak red emission was observed on two occassions by two different workers (A. Tepper and Y. Machi).

II. GROWTH OF SELENIUM AND SELENIUM-TELLURIUM SOLID SOLUTION SINGLE CRYSTALS

(P. Swinehart)

Three methods of growing selenium monocrystals have been tried, Czochralski, vapor phase, and travelling solvent (modified Bridgman). The Czochralski method has the greatest potentiality for the growth of defect-free crystals because the growth interface is free of contact with the container surface. There are other problems with the Czochralski method, however, which make the consistent growing of single crystals difficult. The vapor phase method produces crystals that are too small for some purposes even when good ones are grown. For these reasons the travelling-solvent technique is presently being used.

The travelling solvent technique[(1)] is the least involved and makes the most efficient use of raw materials. About 65 $\sim$ 75% of the Se is usable (grain size on the order of cm). The glassware, shown in Figure 1,* is cleaned in a solution of 5% HF, 60% H_2O, 33% HNO_3 and 2% Alconox solution, rinsed in hot isopropyl alcohol and allowed to dry. The point is cut off the crucible to facilitate cleaning and put back on with a torch afterward. The Se (and Te if alloys are being grown) and Tl are loaded and immediately placed in a 10^{-6} Torr vacuum. Seventy grams of Se make a 1 cm diameter crystal about 10 inches long. Tl in the amount of 1 at .% of the Se is used. Analyses done at Battelle Memorial Institute show that about 400 ppm Tl remains in the crystal.

---

(1) References are located at the end of each section.

* Figure numbers are numbered by chapter.

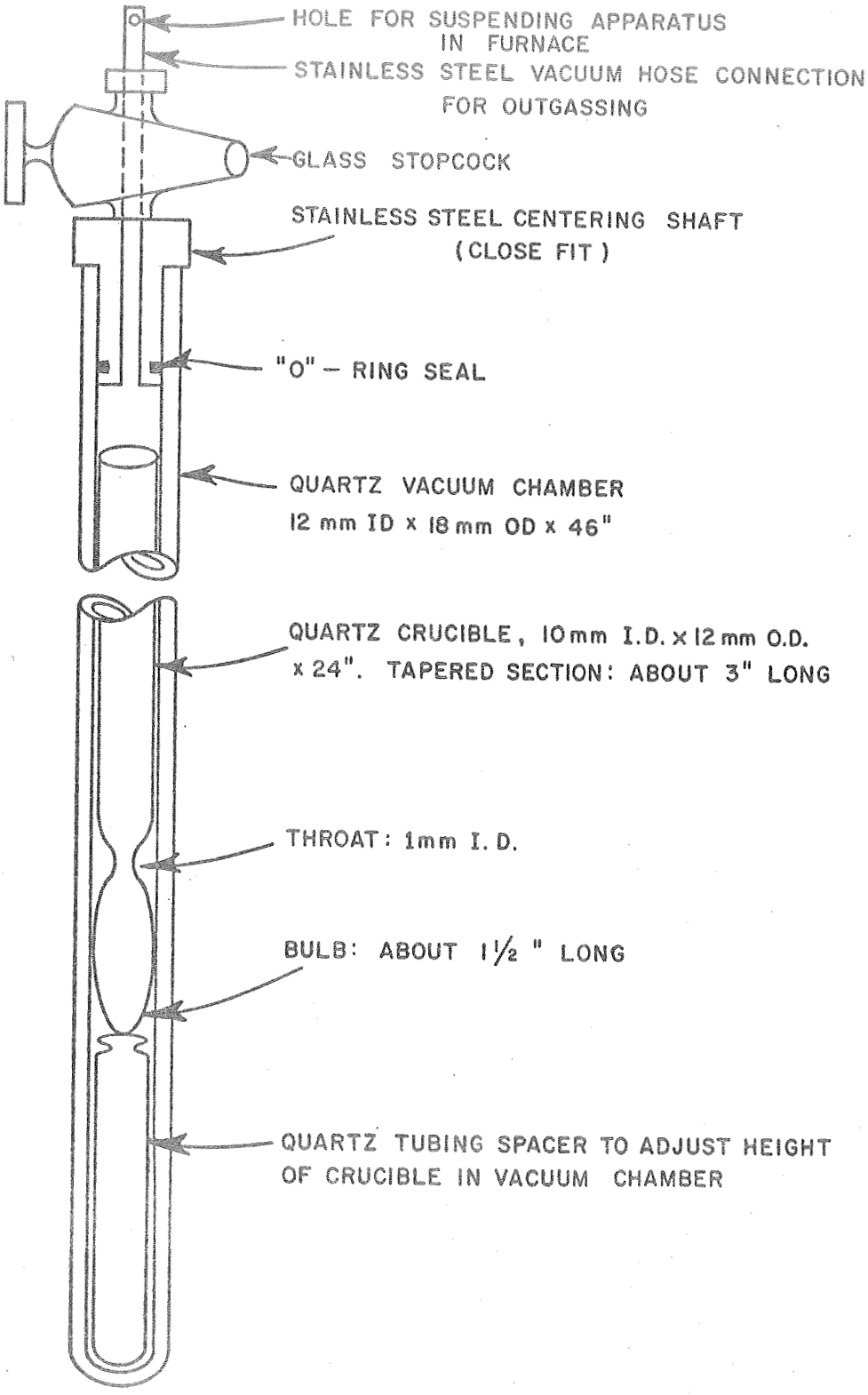

Figure 1. Apparatus for containing selenium for traveling solvent method of crystal growth.

The excess is to take care of losses in initial nucleation and in surface bubbles. A greater concentration of Tl might cause constitutional supercooling.

A cold trap is used between the pump and the crucible. The material is outgassed with a propane torch, starting at the tip and working slowly upward. Tapping the vacuum chamber with a metal object helps to release bubbles. It is difficult to tell when the material is giving off trapped gasses and when it is boiling. Boiling should be avoided because cavitation simply produces more bubbles on the sides. The unmelted material acts as a filter to prevent Se vapor from escaping until all of it is melted. Heating the chamber wall just below the unmelted material allows the Se to drop through a very hot zone as it falls into the melt and most of the gasses are driven out then. The vacuum chamber is sealed when outgassing is completed and hung in the Bridgeman furnace with a fiberglass cord. The crystal is allowed to come to equilibrium for 10 $\sim$ 20 hours before lowering it at speeds of between 0.01 and 0.1 cm/hour.

Temperature control is provided by a Fisher thermistor controller. Additional precautions that may or may not be necessary are enclosing the furnace in a container to control drafts and turning off the air conditioning system in the room.

The growth interface is convex into the liquid. This allows spuriously nucleated crystals to grow into the wall and eliminate themselves. The crystal starts out polycrystalline with very fine grains and improves as the growth progresses. This improvement is shown in Figure 2. Cross section b) is about 1 inch farther along the crystal than a) and c) is another inch

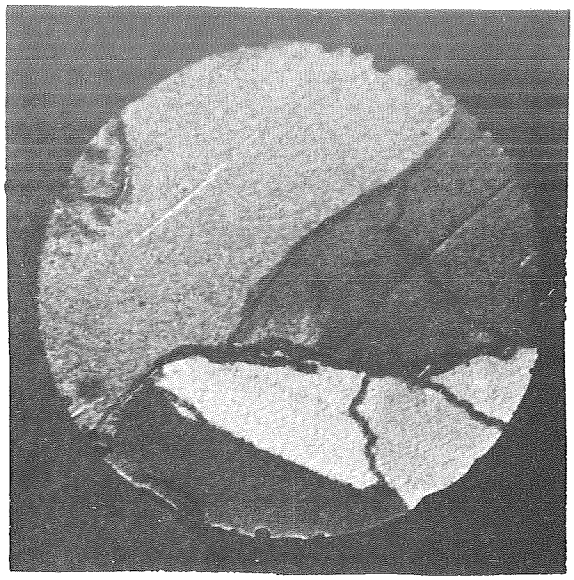

(a)

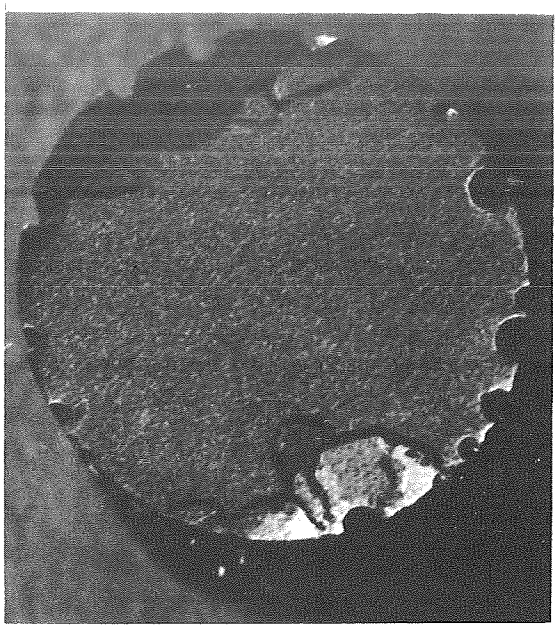

(b)

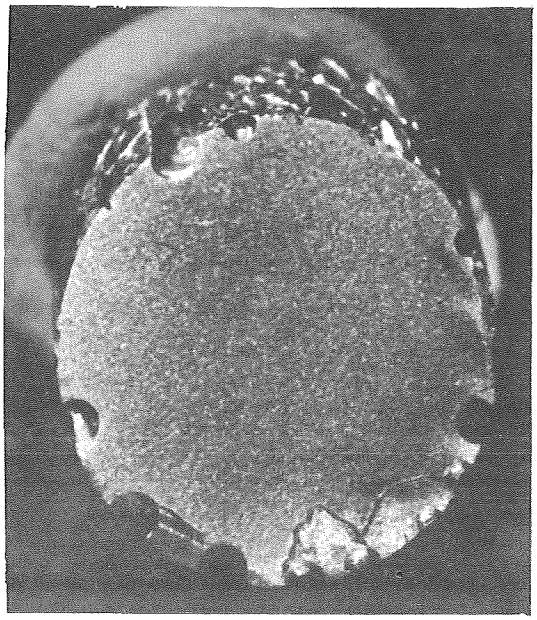

(c)

Figure 2. Cross sections of crystal B-17 etched in Na_2S + H_2O, showing the improvement in the crystal along its length. b) is about 1" farther along than a), and c) is another inch along. The grains are outlined in pencil for photographing. The two small grains in c) are superficial. The cross sections are of 1 cm diameter.

along. Except for a couple of small surface crystals, the boule is entirely single crystalline at c).

Figure 3 shows an $Se_{.75}Te_{.25}$ crystal which displays the edges of the $(10\bar{1}0)$ cleavage planes. Figure 4 is the last crystal grown and apparently the most successful. The pieces in a) are due to natural cleavage due to longitudinal stress in cooling. This can be reduced by reducing the temperature gradient below 170°C from its present value of 35°C/cm.

Figure 4b) is a naturally cleaved $(10\bar{1}0)$ plane of sample B-31-1, which is the section between 6 and 7 cm in Figure 4a). The pattern on the surface is due to strain while breaking and not grain boundaries. Figure 4c) is this surface after lapping and etching in $Na_2S + H_2O$. It shows no grain boundaries and no fine structure under polarized light. There are surface voids visible and two in the bulk. They do not seem to interfer with growth.

The absorption constants of sample B-31-1 with three different surfaces are:

a) natural cleavage $(10\bar{1}0)$ $\alpha = 1.88\ cm^{-1}$

b) natural cleavage etched in $CrO_3 + HCl$ $(10\bar{1}0)$ $\alpha = 7.5\ cm^{-1}$

c) lapped surface etched in $Na_2S + H_2O$ and then in $CrO_3 + HCl$ $\alpha = 13.8\ cm^{-1}$

The temperature was 293°K and $\lambda = 0.95\ \mu$ (unpolarized light) for this sequence of measurements, which shows the problems associated with handling and fabricating the material. The increases in absorption were primarily

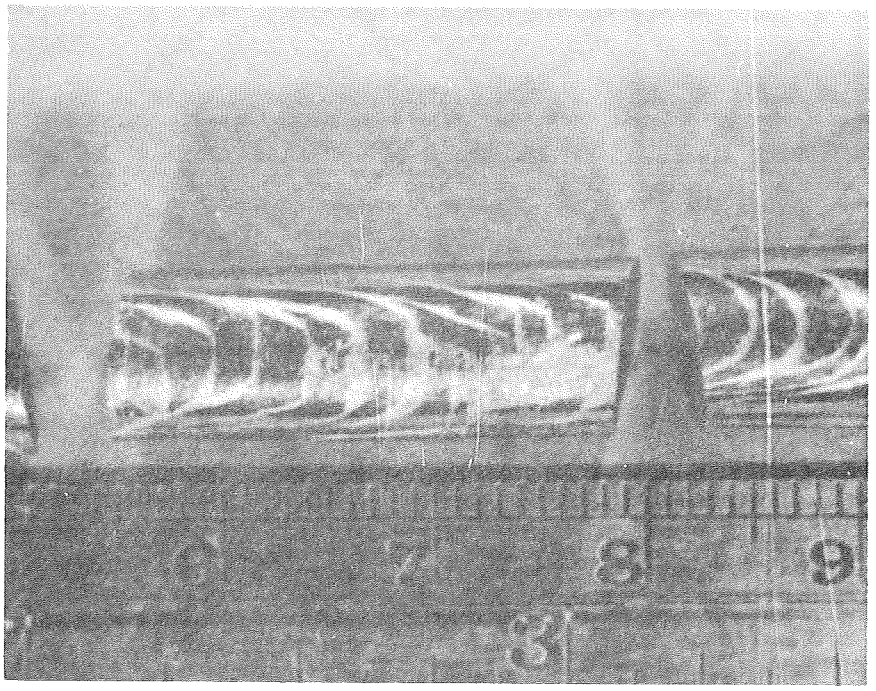

Figure 3. A $Se_{.75}Te_{.25}$ crystal showing the ends of the $(10\bar{1}0)$ cleavage planes. The scale is in cm.

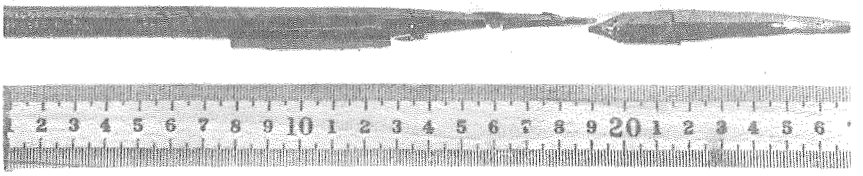

(a)

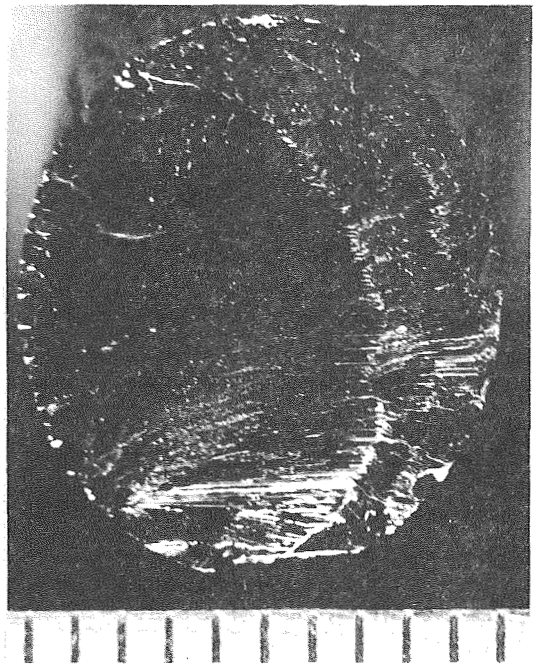

(b)

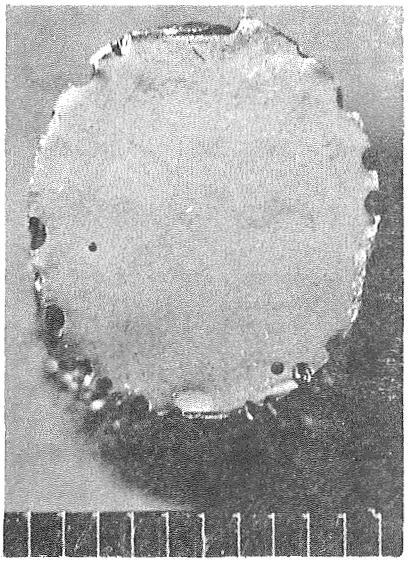

(c)

Figure 4a). Crystal B-31. The crystal is in sections due to longitudinal stress in cooling. One surface of the section (B-31-1) from 6 to 7 cm is shown in b). The failure started in the lower left-hand corner. The surface pattern is not due to grain boundaries as is shown by the lapped and etched section in (c). Surface marks are caused by uneven etching.

due to mechanical damage since the absorption measurements were made by tilting the sample 10° to get a longer distance through the crystal after the first measurement was made perpendicular to the surface (perpendicular to the "c" axis also):

$$\frac{I_1}{I_2} = \frac{I_o}{I_o} \; e^{-\alpha(x_1 - x_2)}$$

where x_1 is the distance perpendicularly through the surface and x_2 is the distance at the 10° tilt. I_o contains the surface effects and is the same for each measurement since the reflectance does not change significantly at small angles.[3] For small angles of tilt ($\theta \sim 10°$), the path difference is approximately, $x_2 - x_1 \overset{\sim}{\sim} x_1 \frac{\theta^2}{2n^2}$.

A 0.5 mm thick slice of sample B-31-1 showed considerably more transmission of red light from a weak source (microscope light) than have previous samples. Very few defects were visible (as dark lines and areas) in this sample as compared to ones from other crystals. See semiannual Status report 2679-2[4] for photographs showing defects when viewed in transmission.

REFERENCES

(1) R. Keezer, C. Wood, and J. W. Moody, Journal of the Physics and Chemistry of Solids, Supplement I, 119, 1967.

(2) E. Sutter, Phys. Stat. Sol. 33, 749, 1969.

(3) T. S. Moss, Optical Properties of Semi-Conductors, Butterworths (London, 1961) pp. 7-8.

(4) Semiannual Status Report 2679-2, Ohio State University Electro-Science Laboratory, July, 1969.

III. PHOTOELECTRIC EFFECTS IN Se_xTe_{1-x} CRYSTALS

(Y. Machi and W. W. Anderson)

In an attempt to determine the defect levels responsible for the relatively large absorption coefficient in Se and Se_xTe_{1-x} alloy crystals, a series of photoconductivity measurements were made. A series of unpolarized spectral sensitivity curves taken at room temperature are shown in Figures 1-4. The first feature to note is the appearance of two maxima in the spectral response curves. The high energy peak in the photoresponse is slightly less than the fundamental absorption edge or band gap in the various alloy compositions. The exact shape of this peak is determined by a number of factors including absorption coefficient, surface condition and sample thickness. The wider photoconductive maximum in the alloy crystals is probably related to the less abrupt absorption edge in these crystals as may be seen by comparing the room temperature absorption spectra of the pure Se crystal shown in Figure 5 and the $Se_{.75}Te_{.25}$ crystal of Figure 6.

The lower energy photoconductive maximum has been observed in Se[1] and Te[2]. However, as improved Te crystals were developed, the low energy peak in Te vanished.[3] It was concluded that the low energy peak was due to a structural defect. If, as we suspect, the low energy peak in Se is also due to a structural defect, it is interesting to note that this structural defect persists through the range of alloy crystals studied to date. From Figures 5 and 6, there is no discernable absorption associated with this photoconductive maximum. In Figure 7, we show the variation, with composition, of the photoconductive peak due to

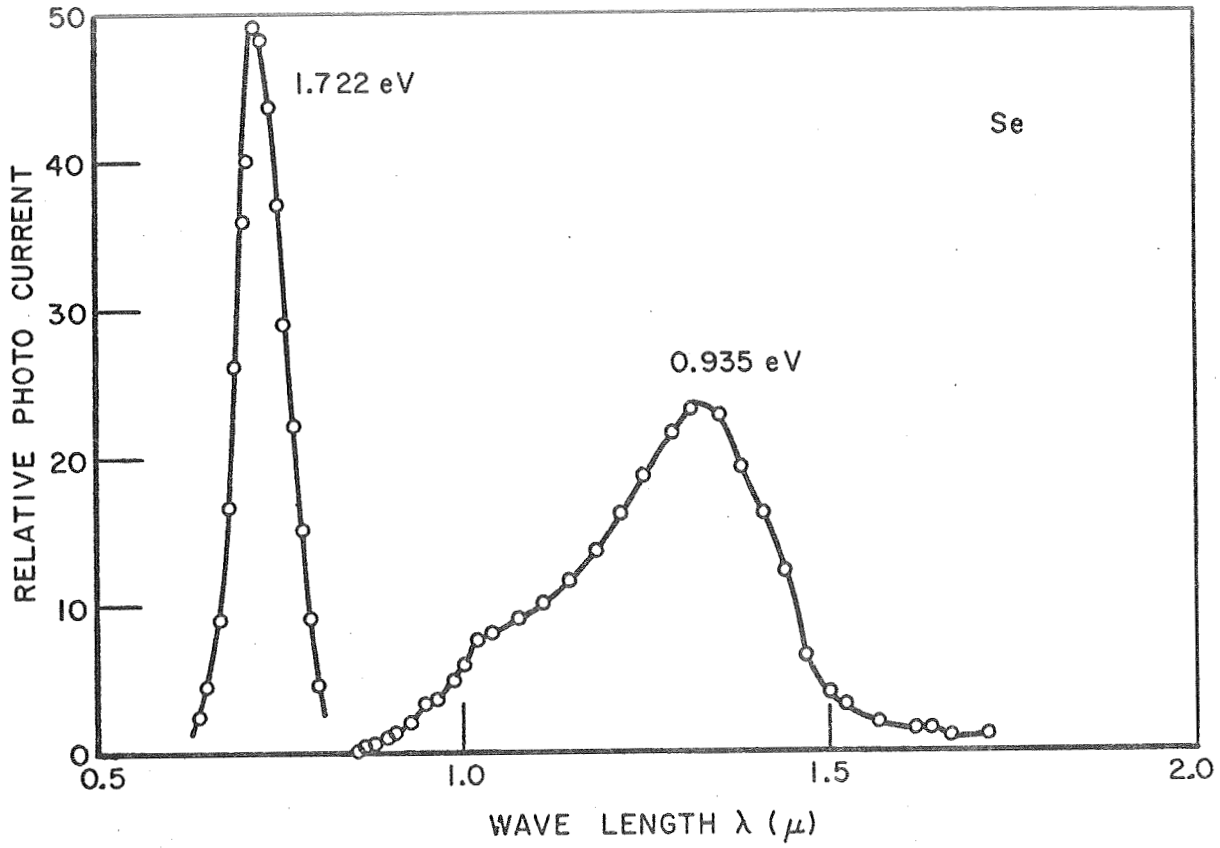

Figure 1. Spectral sensitivity of Se single crystal photoconductivity at room temperature.

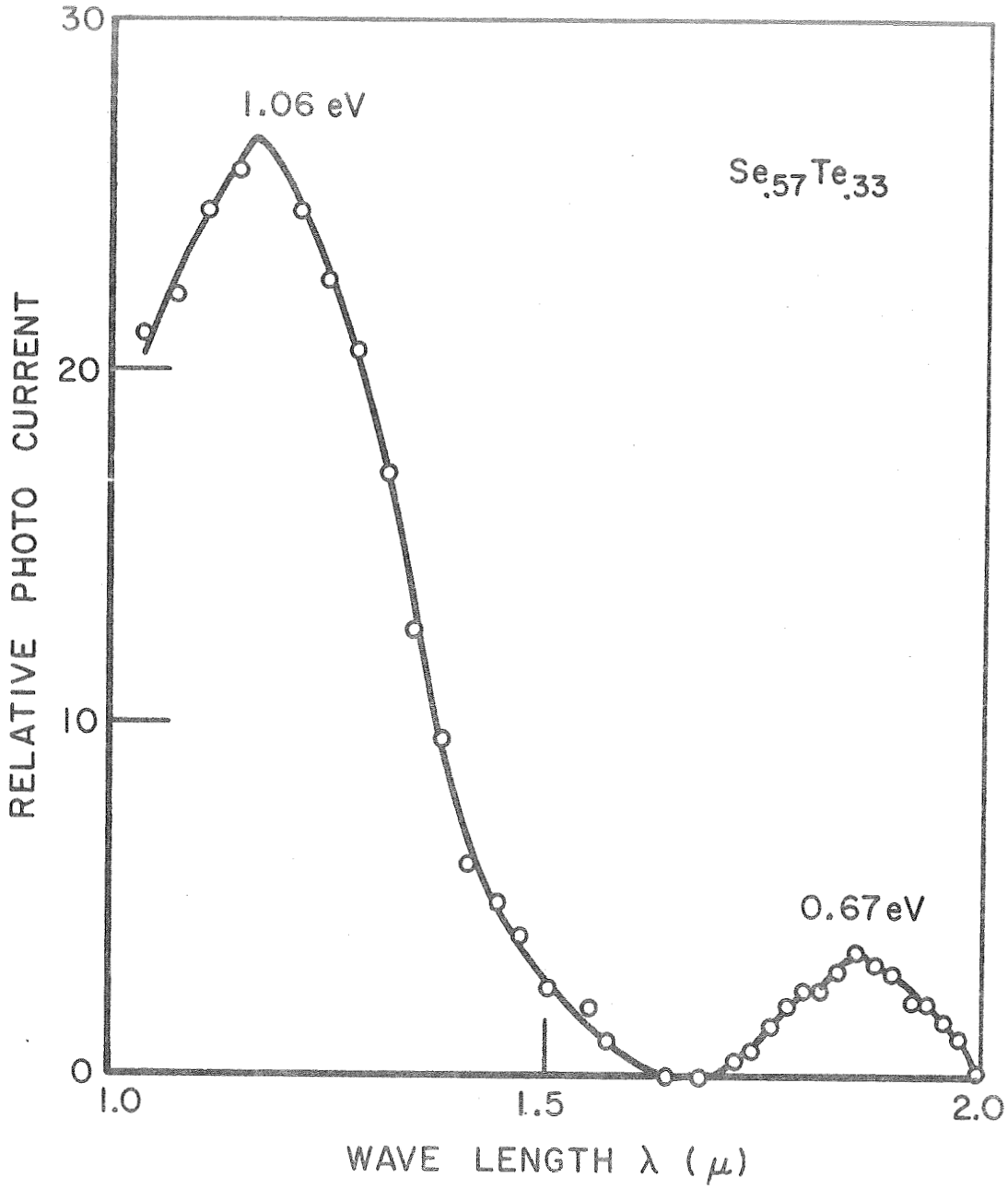

Figure 2. Spectral sensitivity of $Se_{.67}Te_{.33}$ alloy single crystal photoconductivity at room temperature.

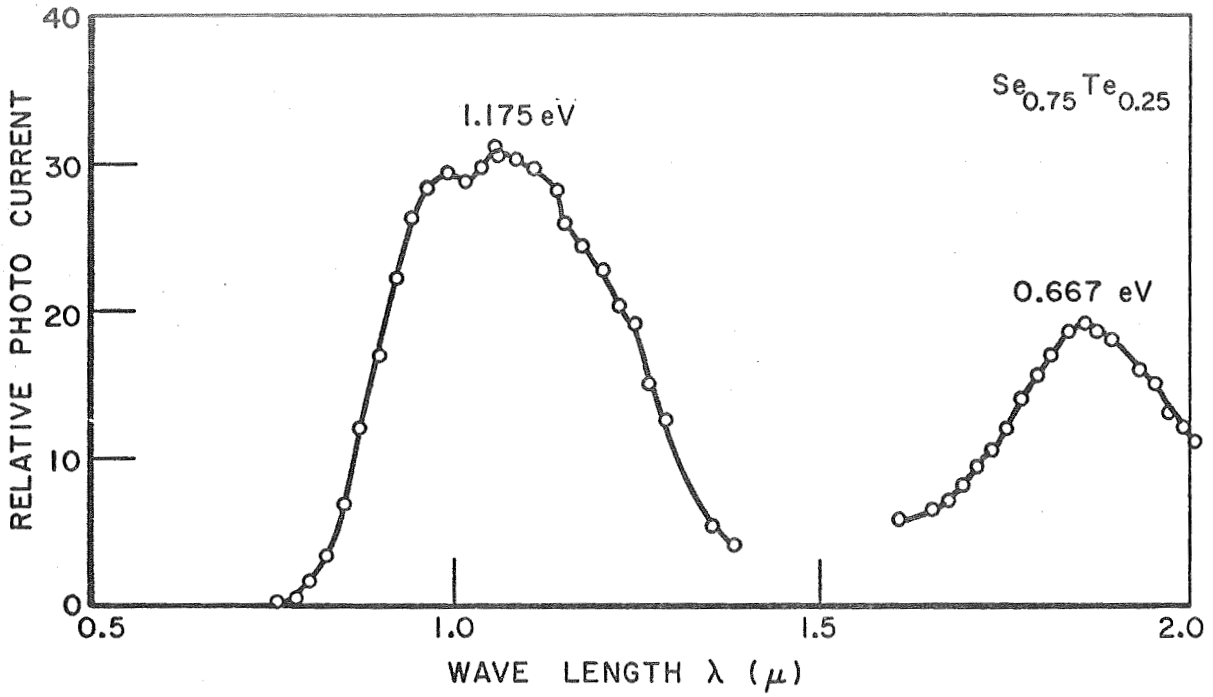

Figure 3. Spectral sensitivity of $Se_{.75}Te_{.25}$ alloy single crystal photoconductivity at room temperature.

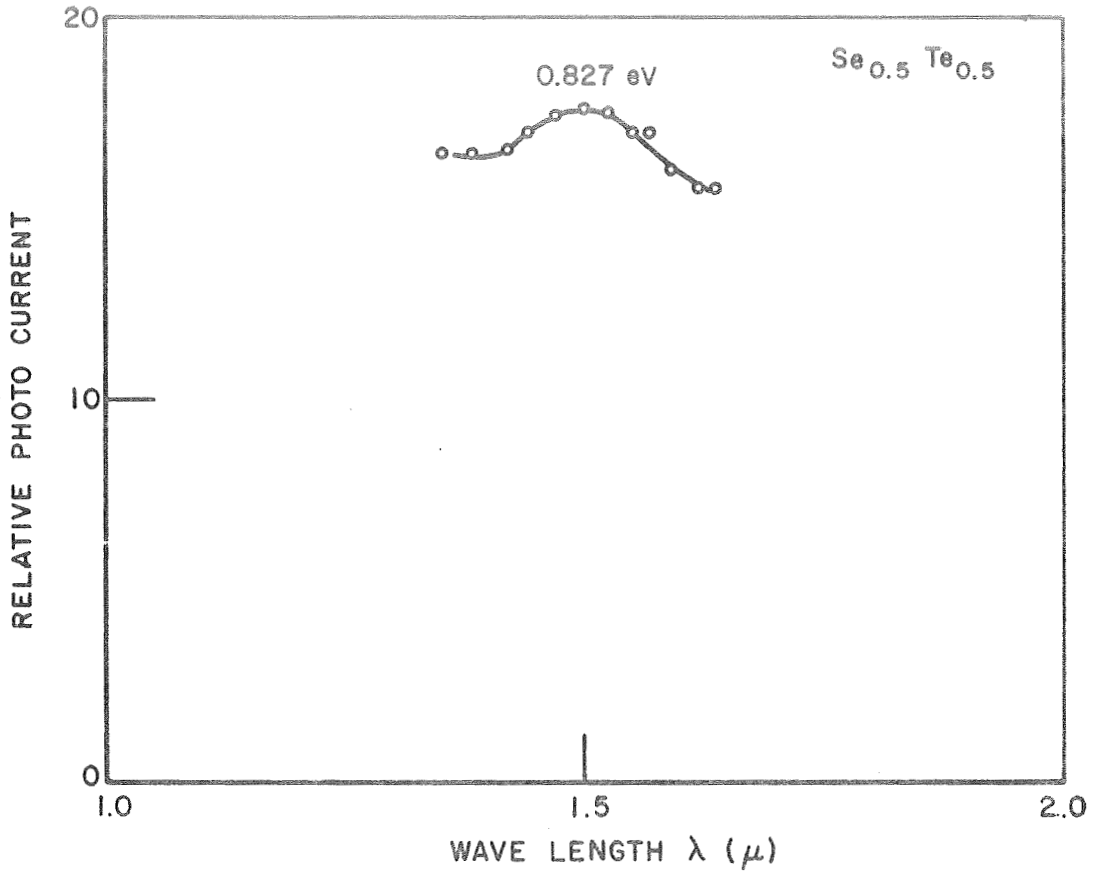

Figure 4. Spectral sensitivity of $Se_{.5}Te_{.5}$ alloy single crystal photoconductivity at room temperature.

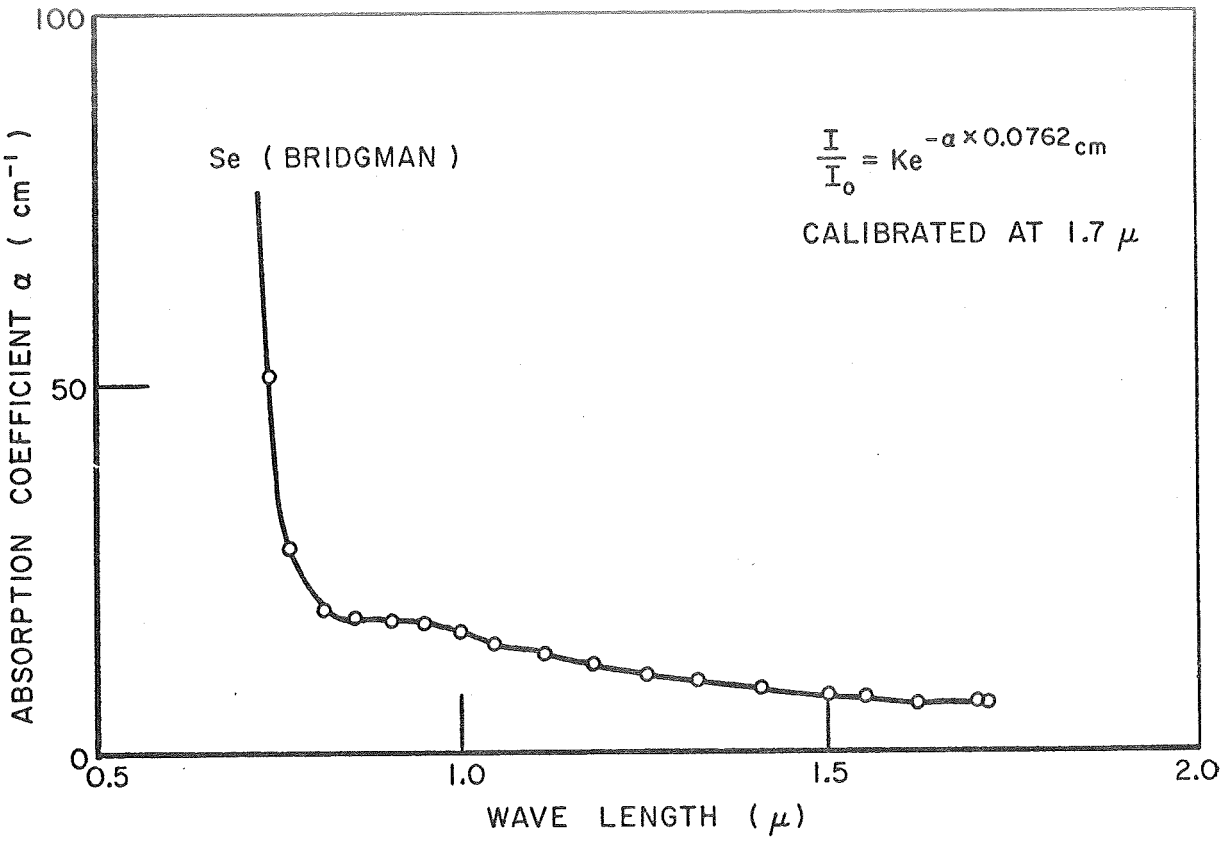

Figure 5. Absorption coefficient for Bridgman grown Se single crystal at room temperature.

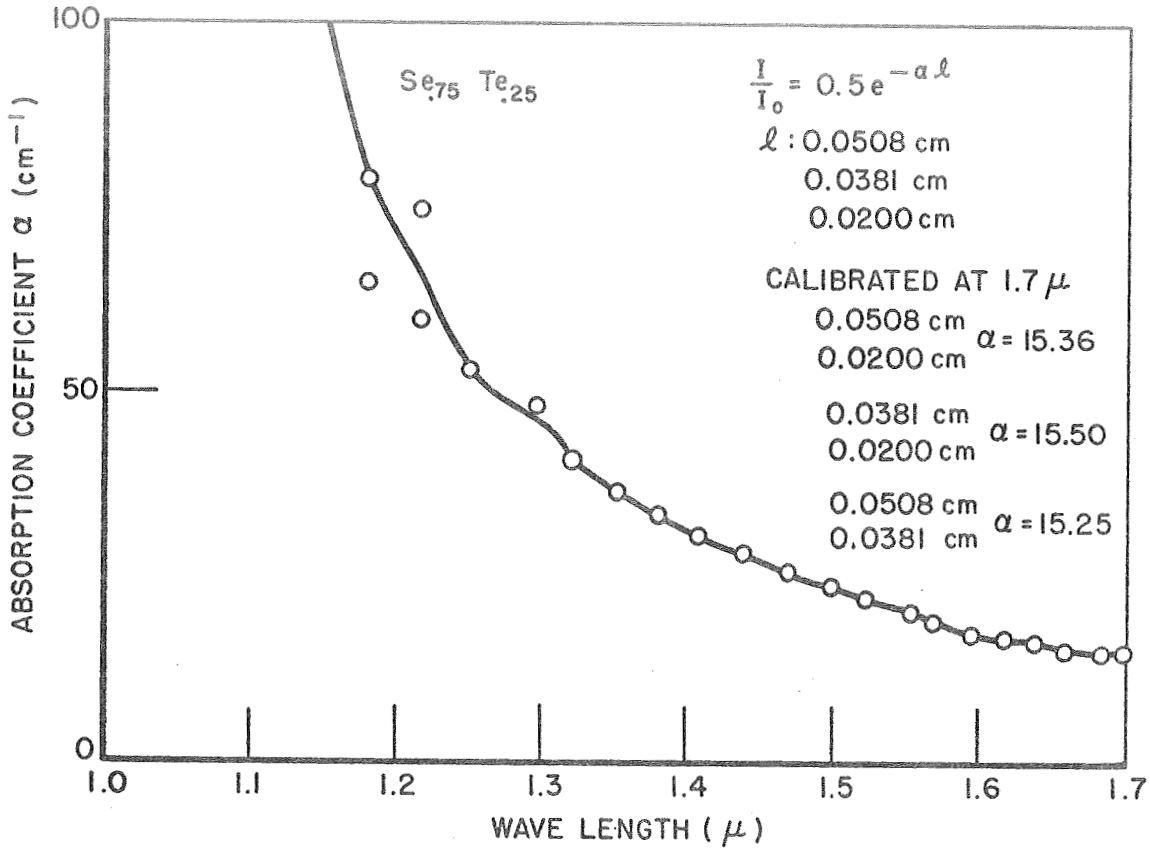

Figure 6. Absorption coefficient of $Se_{.75}Te_{.55}$ alloy single crystal at room temperature.

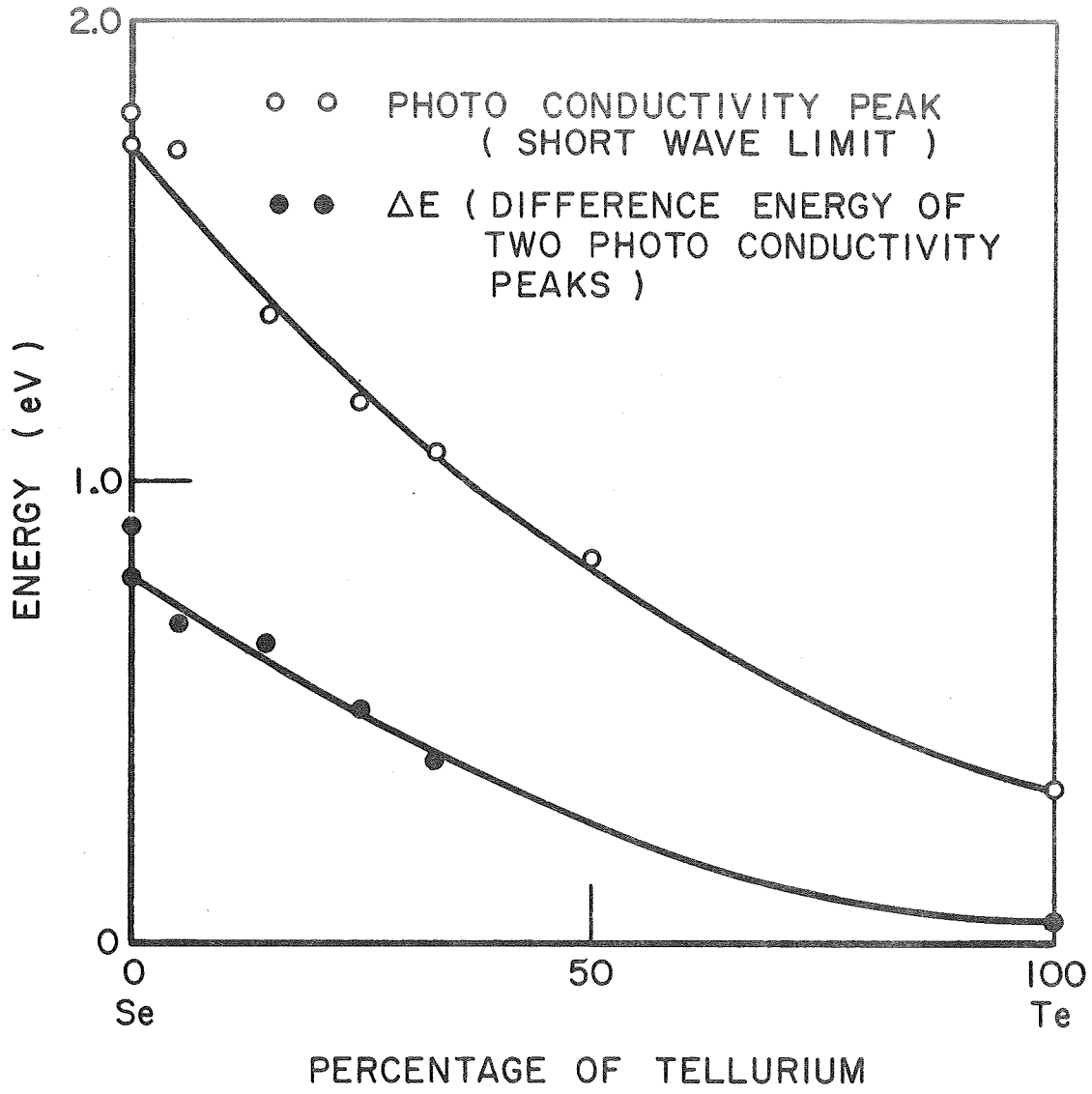

Figure 7. Variation of photoconductive peaks with alloy composition in Se_xTe_{1-x} mixed crystals.

valence to conduction band transitions and the energy separation of the two photoconductive peaks. The upper curve gives the smooth variation of energy gap with composition. The lower curve shows a similar smooth variation of peak separation.

The well known dichroism in the absorption edge of Se[4] and Te[3,5] is reflected in the polarization dependence of the photoconductivity as shown in Figures 8-11. Comparing our photoconductive data in Se at room temperature, Figures 1 and 8, and at 77°K, Figure 12, with published data on the absorption edge of Se[4] and the published photoconductive data on Te[3] with the absorption edge,[5] indicates that the photoconductive maximum occurs at a photon energy where the absorption coefficient is approximately $\alpha \sim 100$ cm^{-1}. We would thus expect the photoconductive peak for $E_{\perp}$ to occur at lower photon energies than the peak for E_{11} and such is indeed the case as can be seen in Figures 9-12. The splitting of the photoconductive peak does not show up for Se at room temperature in Figure 8 since the dichroism of Se at $h\nu = 1.72$ eV ($\alpha \simeq 10^2$ cm^{-1}) is negligible[4]. However, at 77°K, $\alpha = 10^2$ cm^{-1} occurs at appreciably different wavelengths. Te is relatively more dichroic than Se and we see that the splitting of the photoconductive peak at the fundamental absorption edge increases significantly as the Te content of the crystals is increased. There is no good explanation for the polarization dependence of the low photon energy peak available yet.

Finally, we should remark on the significant narrowing of all photoconductive peaks in Se as the temperature is reduced from 300°K (Figures 1 and 8) to 77°K (Fig. 12). This is to be contrasted with other workers who report no narrow bands in the spectral dependence of photoconductivity.[1,6,7]

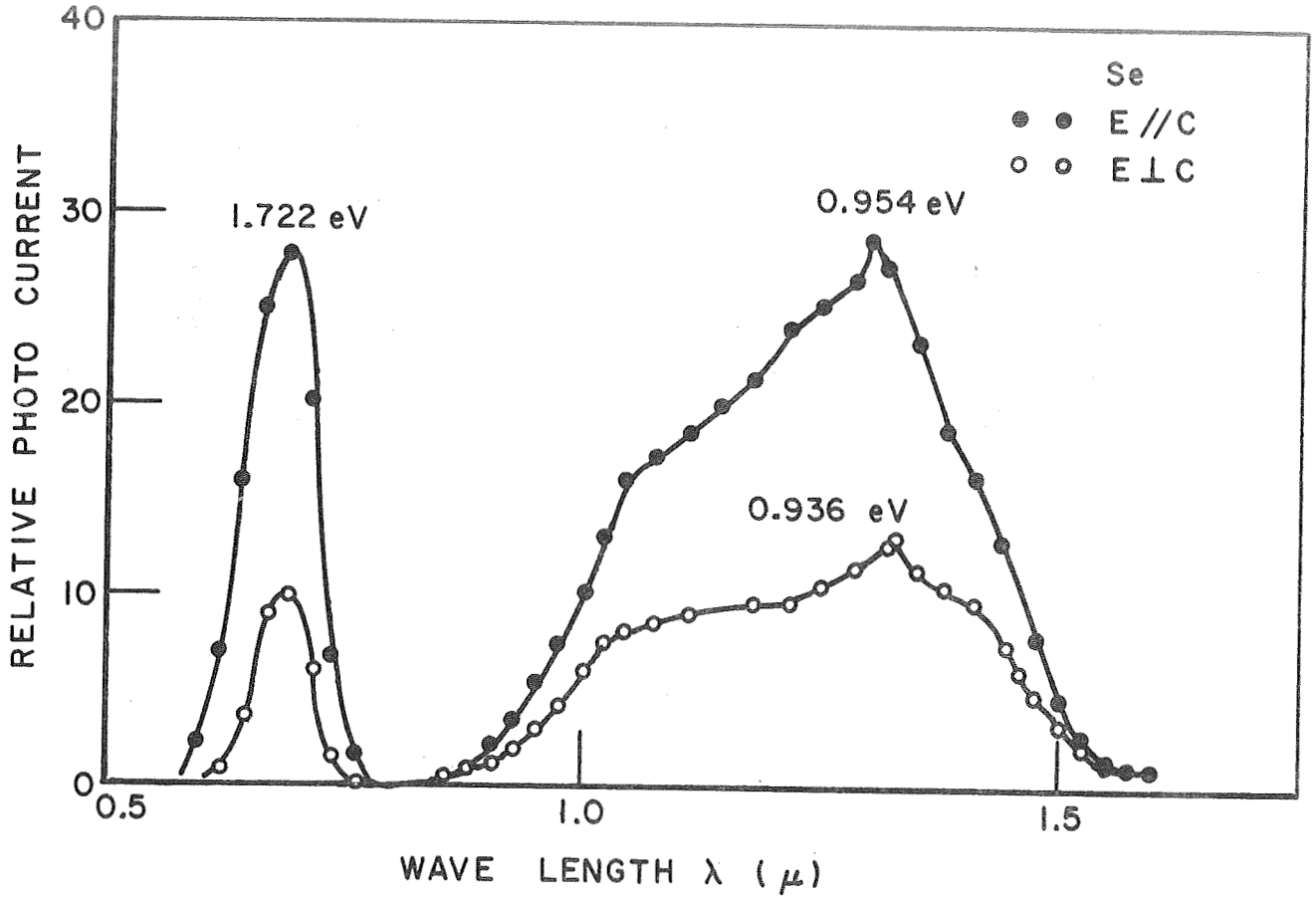

Figure 8. Polarization dependence of photoconductivity in Se single crystal.

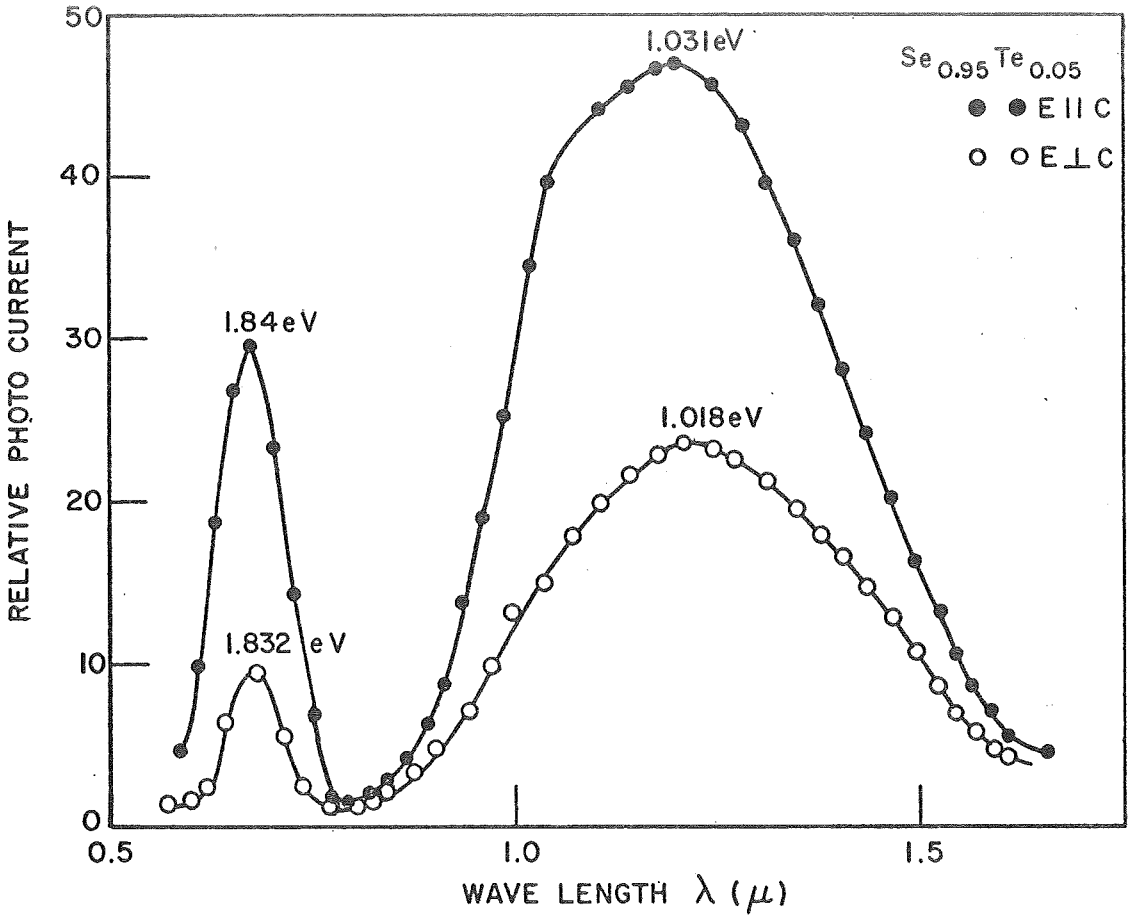

Figure 9. Polarization dependence of photoconductivity in $Se_{.95}TE_{.05}$ alloy single crystal.

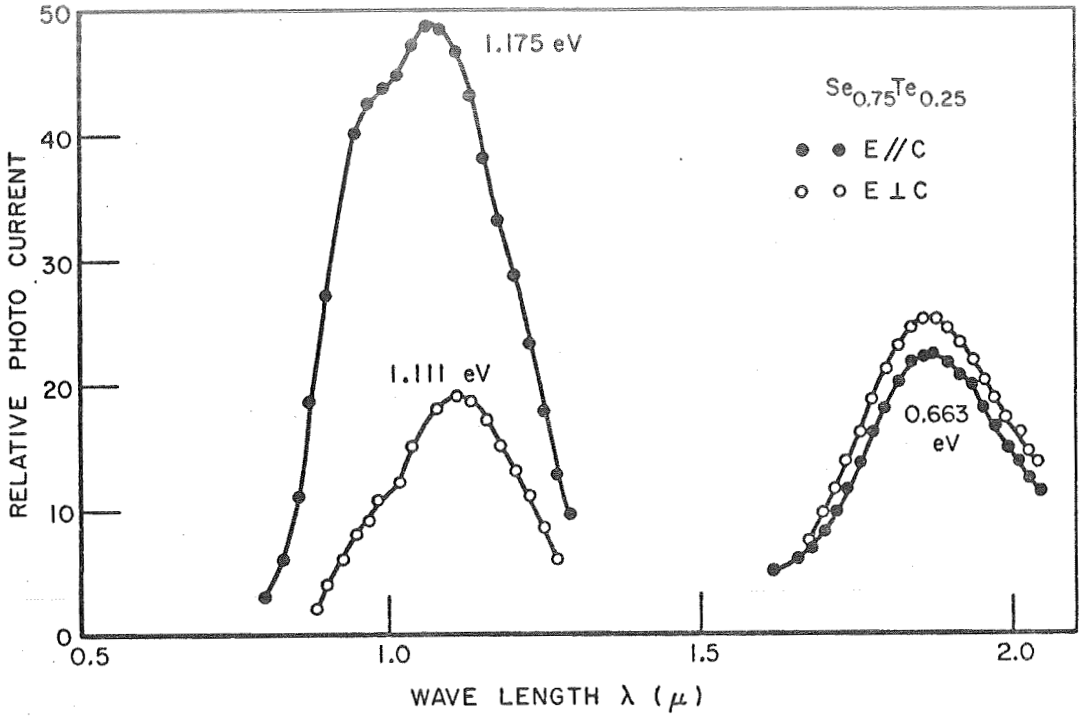

Figure 10. Polarization dependence of photoconductivity in $Se_{.75}Te_{.25}$ alloy single crystal.

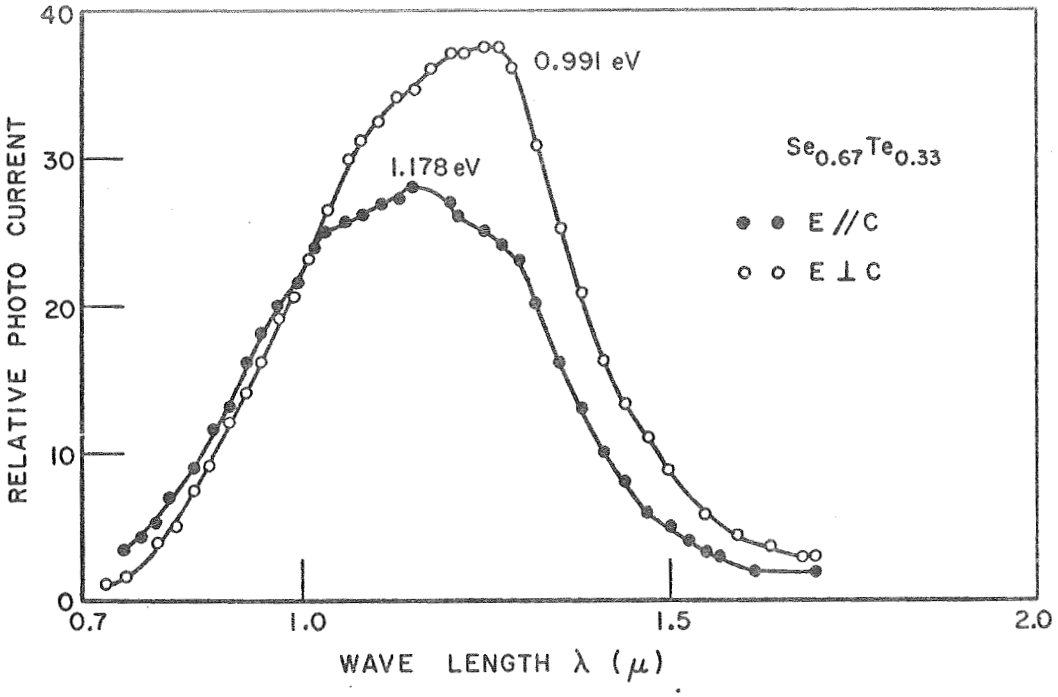

Figure 11. Polarization dependence of photoconductivity in $Se_{.67}Te_{.33}$ alloy single crystal.

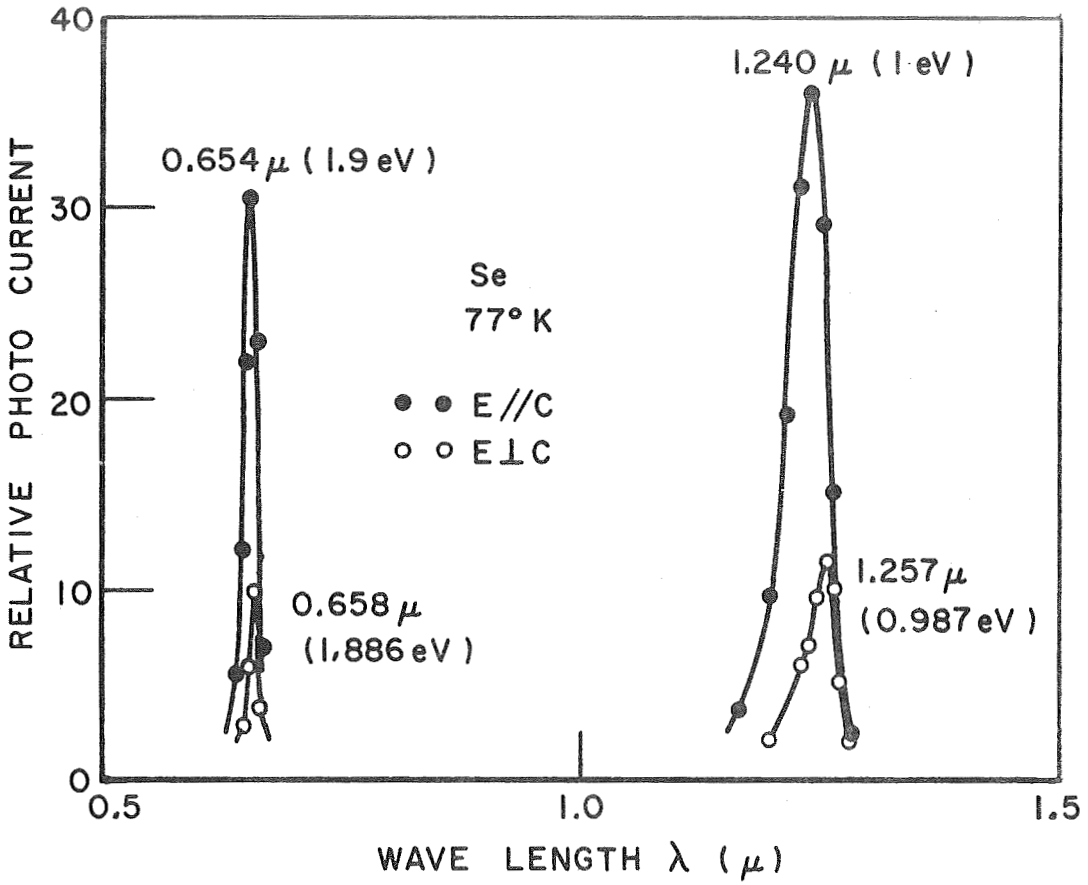

Figure 12. Photoconductive sensitivity spectrum of Se single crystal at 77°K.

LIST OF FIGURES

FIGURE

REFERENCES

(1) J. Stuke, Phys. Stat. Sol. 6, 441 (1964).

(2) J. J. Loforski, Phys. Rev. 93, 707 (1954).

(3) J. S. Blakemore, D. Long, K. C. Nomura, and A. Nussbaum, Progress in Semiconductors, Vol. 6, 39 (J. Wiley and Sons, 1962).

(4) G. G. Roberts, S. Tutihasi, and R. C. Keezer, Phys. Rev. 166, 637 (1968).

(5) J. S. Blakemore and K. C. Nomura, Phys. Rev. 127, 1024 (1962).

(6) S. O. Hemilä and T. O. Tuomi, Ann. Acad. Sci. Fenn. Series A VI, 199 (1966).

(7) S. O. Hemilä, Ann. Acad. Sci. Fenn. Series A VI, 323 (1969).

IV. THERMALLY STIMULATED CURRENTS IN Se_xTe_{1-x} SINGLE CRYSTALS

(Y. Machi and J. Shea)

The work on thermally stimulated currents in Se, described in Semiannual Status Report 2679-3 of this grant,[1] was extended to the alloy crystals and some superior pure Se crystals.

Other workers have observed very complex thermally stimulated current (T.S.C.) spectra in Se[2,3,4]. As our crystals have improved, the observed spectra have simplified. Thus, the two peaks occurring between T = 85°K and T = 115°K in reference (1) are greatly reduced or missing from some of our recent crystals. The results of several T.S.C. measurements are summarized in Table 1.

While the data of reference 1 was analyzed by the initial slope method[5], the data of this report was analyzed by the variation of heating rate method[5]. The close agreement of the results from the two methods should be noted for Se.

The deeper trap levels observed for the alloy crystals probably indicates the cruder state of crystal growing technique to date for the mixed crystals as compared to pure Se single crystals. This may also account for the wider photoconductivity peaks in the mixed crystals.

TABLE 1

TRAP LEVELS IN Se_xTe_{1-x} CRYSTALS DETERMINED BY T.S.C. MEASUREMENTS

Crystal	Se	$Se_{.95}Te_{.05}$	$Se_{.75}Te_{.25}$	$Se_{.67}Te_{.33}$
	.0275 eV	--	--	--
	.0347 eV	--	--	--
	--	--	--	.0404 eV
	.0533 eV	.0535 eV	.0566 eV	.0566 eV
Energy	--	--	.0643 eV	--
	--	--	.0777 eV	--
	--	--	.119 eV	.119 eV
	--	.13 eV	--	--
	--	.138 eV	--	.150 eV

REFERENCES

(1) J. Shea, Semiannual Status Report 2679-3, Ohio State University Electroscience Laboratory, 16 January, 1970.

(2) H. K. Henisch and M. H. Engineer, Phys. Letters 26A, 188 (1968).

(3) S. O. Hemilä and T. O. Tuomi, Ann. Acad. Sci. Fenn. Series A VI, 199 (1966).

(4) T. O. Tuomi, Acta Polyt. Scand. Physics incl. Nucleonics Series 56, Helsinki, 1968.

(5) K. H. Nichols and J. Woods, Brit. J. Appl. Phys. 15, 783 (1964).

V. PHASE MATCHING FOR SECOND HARMONIC GENERATION IN Se AND Se_xTe_{1-x} CRYSTALS

(W. W. Anderson)

The large birefringence and small dispersion in both Se and Te in the wavelength range 10.6 μm to 5.3 μm result in phase matched second harmonic generation for signals propagating very nearly parallel to the c-axis. ($\theta_m = 6°$ in Se and $\theta_m = 14°$ in Te.)[1] However, it is very difficult to prepare crystals with flat, polished entrance surfaces perpendicular to the c-axis due to the weak bonding parallel to the c-axis. Optically good surfaces can be formed on the $(10\bar{1}0)$ cleavage planes as shown in Section II of this report. However, it is not possible to couple energy in at the phase matching angle through this surface, even for glancing incidence.

Recently, the problem of coupling into thin film wave guides was solved by fabrication of a diffraction grating on the surface of the film.[2] A similar technique may be used for coupling into a wave propagating at $\theta_m \simeq 6°$ by near normal incidence (say $\phi_i \simeq 20°$) on a $(10\bar{1}0)$ plane. The appropriate relation is

$$\sin (90° - \theta_m) = \frac{1}{n_o} \sin \phi_i + m \frac{\lambda_o}{a n_o}$$

where $\phi_i \equiv$ angle of incidence

$n_o \equiv$ ordinary refractive index

$\lambda_o \equiv$ free space wavelength

$a \equiv$ grating periodicity

$m \equiv$ order of diffraction

For near normal incidence (but not $\phi_i = 0$ to avoid excitation of m = 0 diffraction mode), most of the energy will be coupled into the m = 1 mode. Large angles of incidence (glancing incidence) result in large reflection loss. As an example, choose $\phi_i = 20°$ and m = 1 for $\lambda_o = 10.6$ μm. For Se, we find a = 4.3 μm. This grating periodicity can easily be fabricated by the photolithographic technique described in reference[2].

REFERENCES

(1) J. Jerphagnon, E. Batifol and M. Sourbe, C. R. Acad. Sci. Paris, 265, Series B, 400 (1967).

(2) M. L. Dakss, L. Kuhn, P. F. Heidrich, and B. A. Scott, Appl. Phys. Letters 16, 523 (1970).

APPENDIX I

CATHODOLUMINESCENCE IN MONOCRYSTALLINE SELENIUM

(A Thesis prepared by A. Tepper)

CHAPTER I. INTRODUCTION

This thesis discusses an investigation of cathodoluminescence in single crystals of hexagonal selenium at 4.2°K. Strong luminescence has been observed in platelets of cadmium sulfide excited by a beam of electrons with energies of approximately 20 keV. It has not yet been possible to verify the observation of cathodoluminescence in selenium with quantitative measurements, but visual inspection indicates that cathodoluminescence in the red region of the optical spectrum may have already been achieved, using approximately 20 keV electron beams.

It is expected that further progress in this investigation will yield information on the band structure and optical properties of single crystals of hexagonal selenium, and that it may lead to the development of electron beam-pumped lasers using selenium and selenium-tellurium alloy systems as active media.

The effort to observe cathodoluminescence in selenium, with a view towards constructing an electron beam-pumped selenium laser, was inspired, in part, by recent successes in constructing a number of electron beam-pumped lasers.[1,2,3] In particular, the observation of laser action in tellurium[4] at 3.647 microns was encouraging because of the chemical similarity between tellurium and selenium and because of the success of the ElectroScience Laboratory of The Ohio State University in growing selenium single crystal of moderate optical quality. Furthermore, reports of the observation of photoluminescence in monocrystalline selenium[5,6] and theoretical[7,8,9] and experimental[10-12] evidence of a direct bandgap in selenium gave some indication

that observation of cathodoluminescence and laser action in selenium might be possible.

This thesis discusses the theory of luminescence within the band structure model of solids and the theory of cathodoluminescence. An appendix dealing with the principles of focusing a beam of electrons is included.

CHAPTER II. BACKGROUND

Selenium is a Group VI-A element, resembling sulfur and tellurium in its physical and chemical properties. Its atomic number is 34 and its atomic weight is 78.96. Its electronic configuration is 2-8-18-6 and it has oxidation states of -2, +4, and +6. Below its melting point (217°C), selenium (Se) is a p-type semiconductor.

Selenium itself is mildly toxic, but its compounds are quite poisonous. Selenium burns in air to form selenium dioxide and it reacts with acids to form hydrogen selenide, which is extremely poisonous. Selenium forms many halogen compounds and many important organic compounds.

Selenium has three crystalline allotropes and three amorphous allotropes. One monoclinic form, α-monoclinic selenium, which is red, is metastable at room temperature, but changes to a deep red monoclinic form, β-monoclinic selenium, when heated above approximately 115°C. Gray hexagonal (sometimes called trigonal) selenium is the most stable of all forms, crystalline or amorphous, at all temperatures. The most common amorphous form is the vitreous type, which has a black, glassy appearance. It is formed by rapidly cooling molten selenium. When heated above 90°C, it changes to the hexagonal crystalline form. The other amorphous forms are a red powder and a red colloidal sol.

Monocrystals of the gray hexagonal form are investigated in this thesis. This form consists of parallel spiral chains located at the corners and center of a hexagonal array. Each helix has three

selenium atoms per turn, with its axis lying in the direction of the c-axis of the crystal. The forces between atoms within a single chain are covalent in nature, but those between chains are only weak van der Waals forces. A crystal of selenium is therefore susceptible to deformation from shear forces parallel to the chains, which accounts for the delicate nature of selenium crystal surfaces, while the strong intrachain covalent bond explains why selenium crystals cannot be cleaved perpendicular to the c-axis. Furthermore, the crystal planes of hexagonal selenium are parallel to the spiral chains.

The electrical resistivity of selenium varies from 10^2 to 10^{12} ohm-cm and varies not only with the allotrope, but also the conditions under which the selenium was prepared before measurement and under which it was measured. In addition, the presence of nonmetallic impurities in selenium generally reduces its resistivity, while the presence of metallic impurities increases resistivity. Illumination of hexagonal selenium for one millisecond decreases its resistivity by a factor of 10 to 15. The resistivity generally decreases exponentially with increasing temperature, and decreases at higher frequencies and intensities of the applied electric field.

Selenium has a large birefringence. The index of refraction for the ordinary wave is $n_o = 2.78$, while for the extraordinary wave $n_e = 3.48$. Selenium has a large nonlinear optical susceptibility. $X^{(2)} = 2 \times 10^{-7}$ esu, where $X^{(2)}$ is defined by

$$\overline{P} = X^{(1)}\overline{E} + X^{(2)}\overline{E}^2 + \ldots\ldots\ldots$$

Photoluminescence in hexagonal selenium was first reported by Queisser and Stuke[6] (1967). Single crystals of selenium were illuminated with 1.96 eV photons from a helium-neon laser. The luminescent spectrum, which was measured at 20°K, showed strongest luminescence at 1.827 eV, with pronounced but less intense luminescence at 1.849 eV and 1.838 eV.

This investigation was repeated later by Zetsche and Fischer[5] (1969), who also examined the temperature dependence of the luminescence. At 4.2°K, they found the peak luminescent intensity to be at 1.820 eV, and within the temperature range from 2°K to 50°K, the position of this peak increased monotonically with respect to temperature from 1.818 eV to 1.833 eV, respectively.

Theoretical studies by Olechna and Knox[9] and by Treusch and Sandrock[8] have indicated that selenium is primarily a direct bandgap semiconductor. These conclusions were borne out, in part, by the experimental work of Stuke and Keller[10] at room temperature, and of Tutihasi and Chen[11] at 20°K. More recent experimental work by Roberts, et.al.[12] indicates direct transitions for optical absorption with the electric field polarized perpendicular to the c-axis, and indirect transitions for the parallel polarization. These results add support to efforts to obtain lasing in monocrystalline hexagonal selenium, because direct transitions are required to achieve the population inversions necessary for the onset of lasing.

The optical absorption edge is the region of abrupt change in the optical absorption spectrum of a material. It is due to allowed

transitions corresponding to the formation of an electron-hole pair at the extrema of the conduction and valence bands. Thus, the location of the absorption edge in the absorption spectrum of a certain material should indicate the location of greatest luminescent intensity within the luminescent spectrum of that material.

Selenium is opaque in most of the optical region. For wavelengths shorter than about 6900Å, selenium has an absorption coefficient of about 3×10^5 cm^{-1}. Roberts, et.al.[12] have measured the absorption coefficient as a function of incident photon energy at 293°K, 197°K, and 77°K. At these three temperatures, they found the absorption edge to be at 1.65 eV, 1.80 eV, and 1.87 eV, respectively. The absorption edge for incident fields polarized perpendicular to the crystal axis was always at lower energies than for the parallel polarization. The long wavelength absorption coefficient beyond the absorption edge was found to be on the order of 5 cm^{-1} at all temperatures, and was always lower for the parallel polarization than for the perpendicular. This residual absorption is probably due to crystalline imperfections in the crystals available to date.

CHAPTER III. THEORY OF CATHODOLUMINESCENCE

Luminescence is the process by which a material emits radiation, usually in the optical spectrum, due to absorption of energy other than thermal energy. The absorbed energy may be supplied by a photon (photoluminescence), an electron beam (cathodoluminescence), a chemical reaction (chemiluminescence), or by a number of other means. Luminescent spectra provide quantitative information regarding the energy band structure of the host material, as affected by impurities and imperfections which may be present.

In the case of selenium, an electron beam is particularly desirable for exciting the luminescent spectrum because most selenium samples are characterized by relatively high losses and significant surface damage. Cathodoexcitation, with high excitation densities and several microns depths of penetration, can compensate for these difficulties. Cathodoexcitation is also of interest because experimentation with cathodoluminescence is easily extended to investigations of possible laser action in selenium, merely by changing the target geometry.

Luminescence persists after removal of the energy source. The period of persistence dividing fluorescence, which is short-persistence luminescence, and phosphorescence, which is longer-persistence luminescence, has been set arbitarily at 10^{-8} seconds.[13]

The luminescent spectrum, if any, of a given material is usually determined by the type of impurities present. These impurities are often introduced intentionally and are called "activators". A certain activator will produce one spectrum in one luminescent material

and another spectrum, or perhaps none at all, in a different host. Luminescence can occur in a chemically pure crystal if crystal defects are present. These defects may be atomic vacancies or interstitials or grain boundary dislocations. These defects are known as activators also. Of course, no real material is chemically pure and all real crystals contain both defects and impurities, but the mere presence of impurities or defects doesn't guarantee that luminescence will occur.

Whether or not activators are present, the luminescent spectrum is independent of the manner of excitation in all but a few materials. However, if optical exictation is involved, the luminescent frequencies are usually less than the frequency of excitation (Stokes Law). Anti-Stokes radiation, for which the luminescent frequency is higher than the excitation frequency, sometimes occurs.

Luminescence has been observed in solids, liquids, and gases, both organic and inorganic. This thesis will deal only with luminescence in solid crystalline semiconductors, and with cathodoluminescence in selenium, in particular.

Luminescent phenomena in many solids are explained within the band structure concept of solids. When a large number of atoms are brought together to form a macroscopic solid, the highest normally filled energy levels of the individual unexcited atoms are broadened into a valence band and the excited energy levels of the individual atoms are broadened into a conduction band.

It is well known that in a very pure semiconductor at absolute zero temperature, the valence band is completely filled, but the valence and conduction bands are separated by a forbidden band (of energies inaccessible to free electrons) whose width, or bandgap, E_g, is on the order of 1.5 eV for the most common semiconductors. At temperatures above 0°K, it is possible for thermal excitation to raise some electrons in a semiconductor to the conduction band, leaving behind a hole in the valence band.

It is also possible for electrons to be raised to the conduction band by absorption of a photon of energy $hf > E_g$. Whether created by thermal or photoexcitation, the conduction band electrons and valence band holes are free, i.e., they aren't bound together, so they can move independently through the semiconductor transferring charge and energy.

This situation is actually quantum mechanical, but for many purposes, it may be viewed classically, provided that two effective mass parameters are introduced in a valid manner. For the use of these parameters to be valid, the applied external forces on the crystal (electrostatic, magnetostatic, and electromagnetic) must be small perturbations of the periodic electrostatic force which arises from the lattice of atomic kernals (nuclei and nonvalence inner electrons). The periodic crystal forces are incorporated in the effective mass for conduction band electrons, m_e^*, and the effective mass for valence band holes, m_h^*. The perturbational forces then influence the conduction electrons and valence holes as they would ordinary classical particles with the appropriate effective masses.

Besides free holes and electrons, there are two other mechanisms by which energy may be transferred through a crystal. These are phonons and excitons. A phonon is a quantized lattice vibration, which manifests itself macroscopically as heat and sound. Quantitative treatments of electron or hole transitions must take into account the energy and momenta of any phonons involved.

An exciton consists of the interaction between a valence band hole state and a conduction band electron state. If these two states both lie very near their respective band extrema (the lower edge of the conduction band and the upper edge of the valence band) they cause a hydrogenic series of bound states lying directly below the conduction band. Since this electron-hole pair is bound together, it cannot transfer net charge, but it can transfer energy through the crystal by migration.

An exciton may be created by absorption of a photon with energy $hf < E_g$ or by union of a free hole and electron. The exciton absorption and emission spectra consist of lines at energies approximately given by

$$hf = E_g - \frac{G}{n^2}$$

where "G" is the binding energy of the exciton (which arises from coulomb interaction between the electron and hole states) and where "n" is an integer. The lowest exciton absorption line may typically have an energy from $0.75\ E_g$ to $0.9\ E_g$.

It is noted that the excitons described above are of the Wannier type, which best describes matters in semiconductors and other high dielectric constant materials where the exciton is not highly

localized in the material. When the exciton is localized, as it is in molecular crystals, a Frenkel type exciton is involved. This type may be thought of merely as a mobile, excited molecular or atomic state.

When activators are present in a crystal, they introduce energy levels which lie in the forbidden band. These energy levels are localized in the regions surrounding the activators, if the concentration of impurities is low. When a mobile, conduction band electron approaches one of these localized levels, it may emit phonons and enter the lower energy state. Then, if the probability that the electron will be re-excited to the conduction band is greater than the probability that it will recombine with a valence band hole, the localized energy level is called a "trap" for electrons. If the probability of re-excitation is less than that of recombination, it is called a "recombination center". The energy level at which the probability of re-excitation equals the probability of recombination is called the "demarcation level".

The mechanism of re-excitation of electrons to the conduction band is usually thermal, so electron traps are typically within a few kT (1/40 eV at room temperature) below the conduction band. The mechanism of recombination may be coulomb attraction between the bound electron at the recombination center and the valence band hole. It is clear, then, that whether or not an activator site acts as a trap or recombination center depends upon the temperature. At higher temperatures, activator sites with energies farther below the conduction band act as traps.

The recombination transition of the electron to the valence band may be either radiative or nonradiative. If it is radiative, the activator site is called a "luminescent center". If not, the energy of the excited electron is released entirely as phonons.

Fluorescence in a semiconductor, then, is the emission of radiation from a luminescent center due to the recombination of electrons and holes. The electrons and holes may have originally been free or they could have been bound excitons.

Phosphorescence in a semiconductor involves trapping and thermal release of conduction band electrons in addition to recombination. Trapping delays the recombination process and causes persistence.

Cathodoluminescence is initiated by directing a beam of electrons at a target, which in this case is a sample of monocrystalline hexagonal selenium. The energy of the incident electron beam is usually above 15,000 eV. Free electron-free hole pairs may then be created by absorption of one of the beam electrons. The efficiency of hole-electron pair production approaches 33%[14], and the bandgap in selenium is approximately 2 eV. Since from two to four times the energy gap is required to create an electron-hole pair, about a thousand electron-hole pairs are created per incident electron.

In the case of selenium, cathodoexcitation is desirable because a focused beam of electrons can provide a high excitation density to a small surface area of the target. For example, Hurwitz indicated the use of electron beams which provided power densities of about 60 kilowatts/cm^2 to areas of about .002 cm^2.

Thus detectable levels of luminescence may be excited in spite of the low external luminescent efficiency of most selenium samples. The external luminescent efficiency, which is the percentage luminescent power output of the total power input, may be low because the localized energy levels associated with impurities or defects act as nonradiative recombination centers. Nonradiative transitions attenuate luminescence and may even eliminate it in regions of the crystal where they predominate over radiative transitions. Since the electron beam can be made to scan the surface of the target, it can be steered away from these regions of lower luminescent intensity until a region of maximum luminescent intensity is found.

In addition, cathodoexcitation is desirable because of the penetration depth of the electron beam. The selenium target is either cleaved out of a larger specimen of monocrystalline selenium, or it is cut out of it and etched. In either case, there is some degree of surface damage to the surface of the target which is exposed to the electron beam. However, a sufficiently energetic electron beam can penetrate below this layer of surface damage and excite luminescence from the more perfect crystal lattice below it. Anderson's method[15] indicates that a 25 keV beam of electrons would activate a region up to about 2.5 microns in depth in selenium, whereas a beam of 1.475 eV photons would activate a region to a depth of about 0.1 micron.

Besides nonradiative transitions, the external luminescent efficiency may be lowered by a number of other factors. For instance,

a substantial fraction of the primary (incident) electrons directed at the target is backscattered, i.e., reflected from the vacuum-selenium boundary. The backscattering coefficient of selenium was found by Palluel[16] to be about 0.35, relatively independent of the primary beam energy. Primary electrons which do penetrate into the crystal may excite secondary electrons which escape from the target or they may excite lattice vibrations, i.e., they may merely heat the crystal.

In addition to these inefficiencies, internally generated luminescence may be internally absorbed if the crystal has a high absorption coefficient at the luminescent wavelength or it may be internally reflected at the air-crystal interface if there is a large index of refraction difference across the interface.

CHAPTER IV. EXPERIMENTAL PROCEDURE

Attempts have been made to observe cathodoluminescence in monocrystalline selenium at liquid helium temperature. A sample of monocrystalline selenium was placed in thermal contact with a liquid helium dewar and maintained at a potential of 15 kilovolts, positive with respect to ground, as shown in Figure 1. The dewar, sample and electron gun are enclosed in a vacuum system capable of vacuums better than 10^{-6} torr. An external micrometer leveling arrangement allows the beam to scan the crystal surface.

The electron gun, of the type used in the 7NP4 projection kinescope, is operated in a pulsed mode at pulse repetition frequencies of one hundred to one thousand hertz and a pulse duration of one microsecond. This is done by applying positive pulses of 300 volts to the control grid, which is normally biased to cut off cathode current, as shown in Figure 2. The cathode is at approximately five kilovolts, negative with respect to ground. Its exact potential is determined by beam focusing requirements, which are discussed in the Appendix. The pulse transformer shown in Figure 2 has been specially wound to stand off 10 kilovolts, in order to protect the pulse generator from this high D.C. voltage. The transformer steps up an 80 volt pulse from the generator to 300 volts, which is applied to the control grid. The pulsing circuit is more completely shown in Figure 3.

When the beam is on, it is accelerated through 500 volts by the first accelerator, shown in Figure 2, and focused by the lens formed

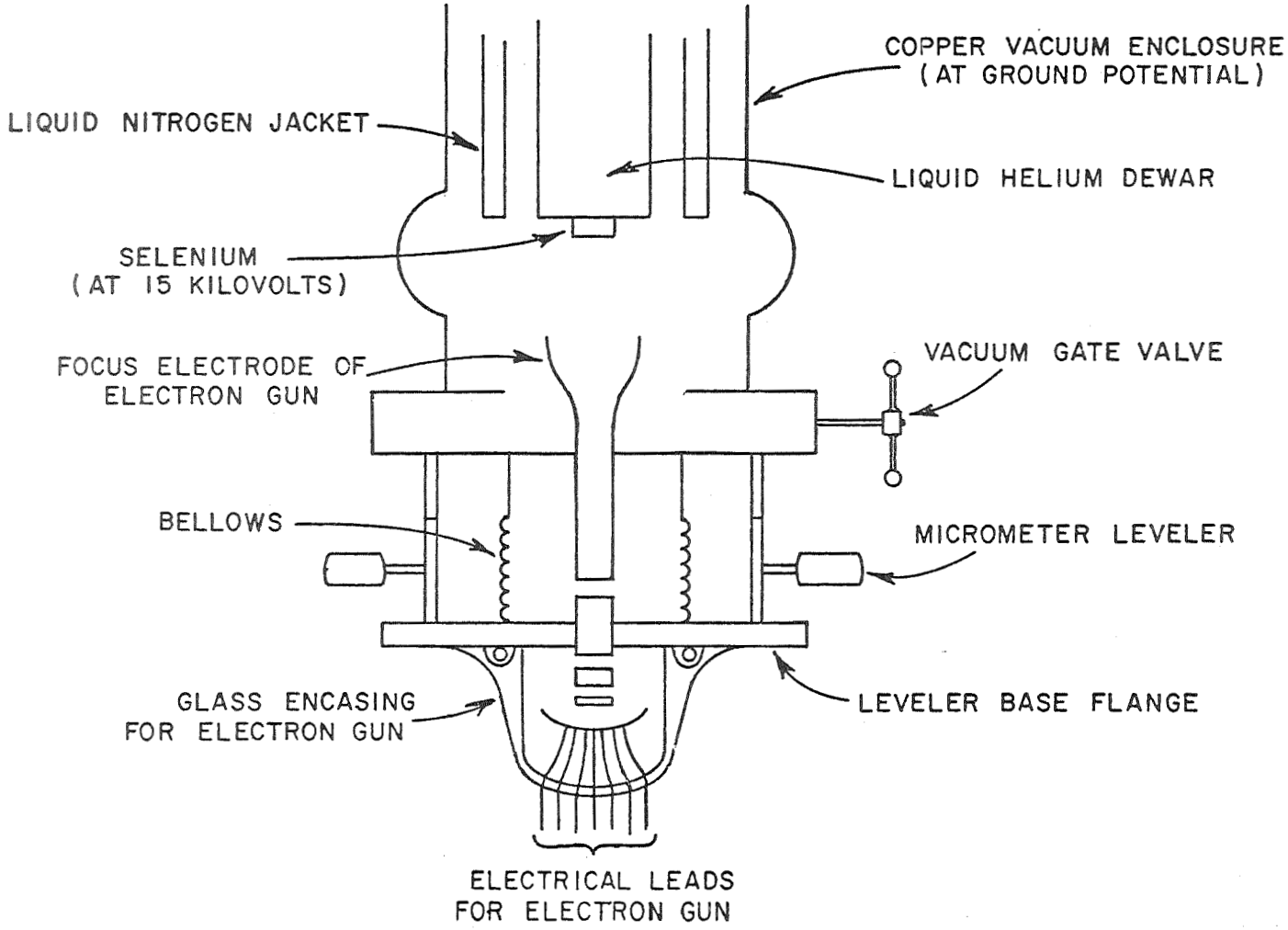

Figure 1. Work Area of Apparatus for Observation of Cathodoluminescence in Selenium at 4.2°K.

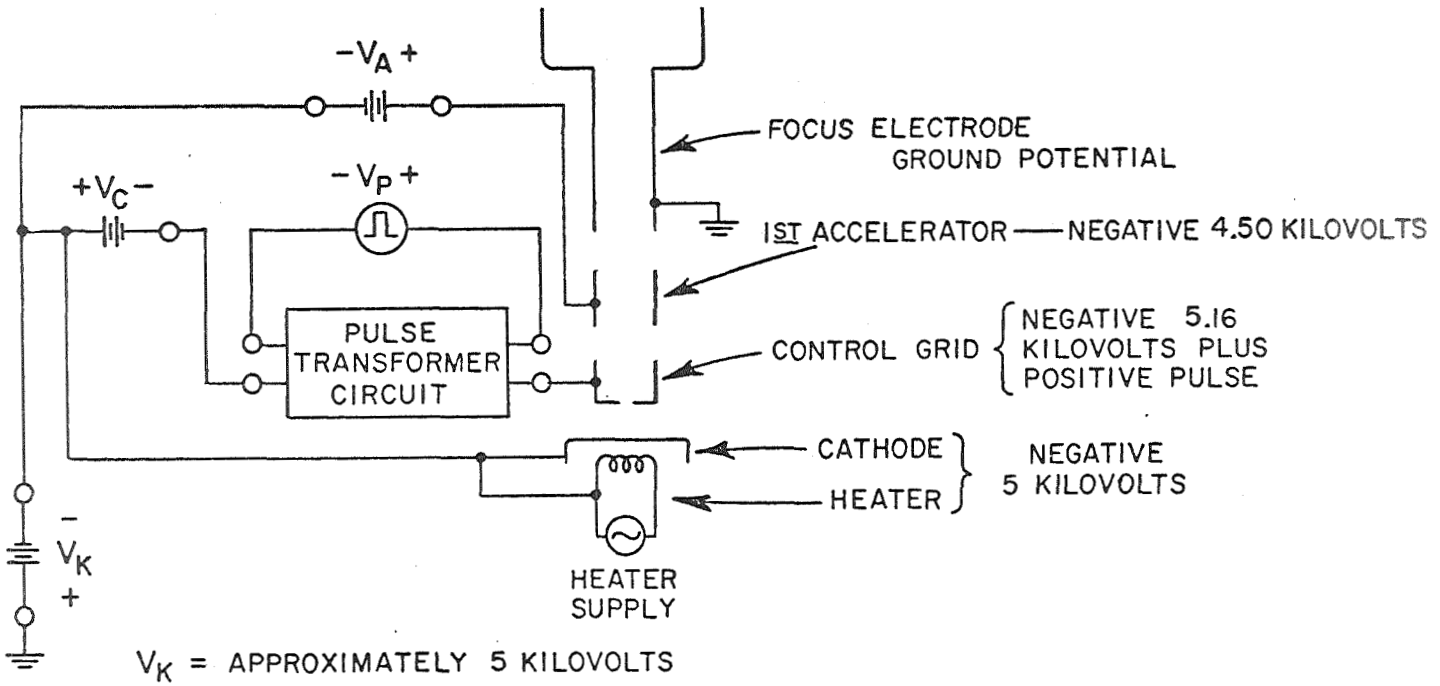

V_K = APPROXIMATELY 5 KILOVOLTS

V_C = 160 VOLTS

V_A = 500 VOLTS

V_P = 300 VOLTS

HEATER SUPPLY = 9.6 VOLTS , 600 ma

Figure 2. Biasing and Pulsing Arrangement of Electron Gun, Showing Typical Voltages.

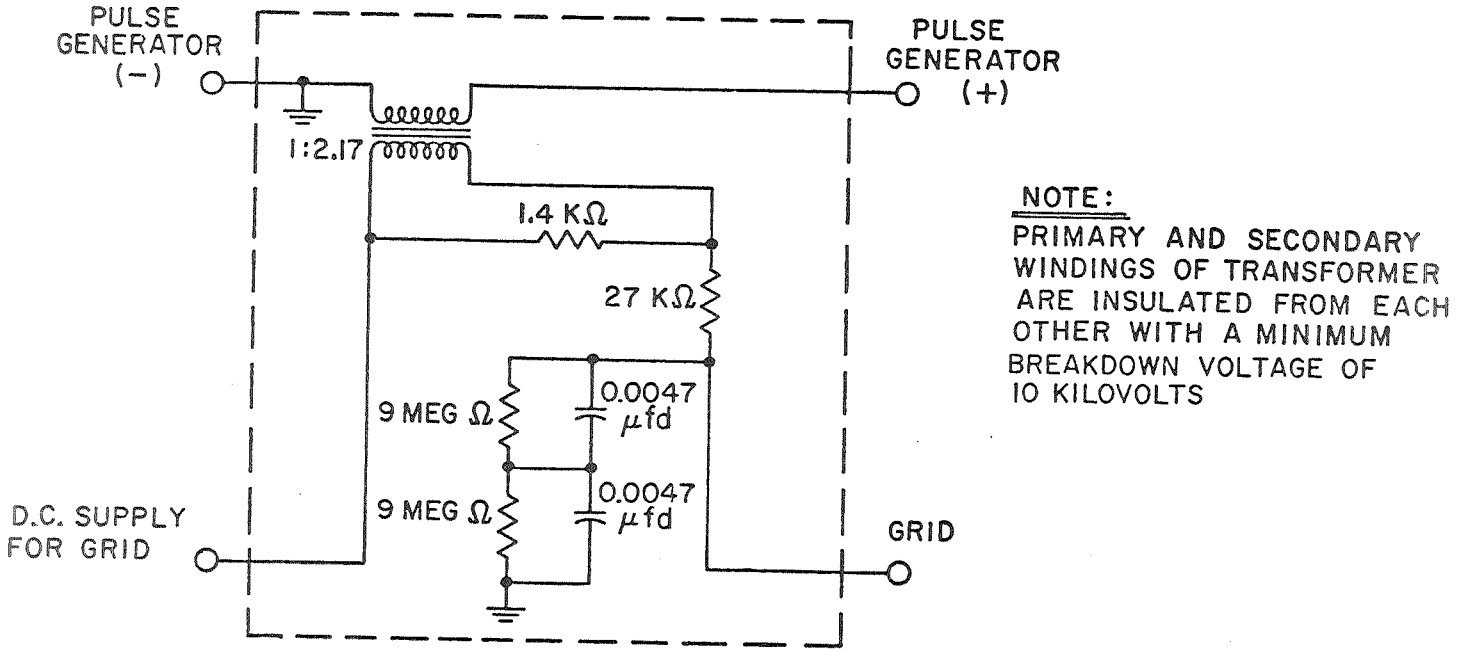

Figure 3. Details of Pulse Transformer Circuit.

between the cathode, the control electrode, and the first accelerator. The beam is refocused and further accelerated as it enters the focus electrode region. The focus electrode is at ground potential. Final acceleration and focusing is obtained as the beam enters the high voltage region. This consists of a glass tube with an aluminum coating vaporized on its inside surface, as shown in Figure 4. This aluminum coating is approximately ten cm long and is at the anode voltage of about 15 kilovolts. This aluminum layer extends about 3 cm below the mouth of the focus electrode and extends up to the target area.

When a selenium sample is removed and the vacuum broken, the electron gun must be maintained at a high vacuum to protect its special oxide cathode. To do this, the bellows arrangement shown in Figure 1 is used. The end of the focus electrode, which extends above the vacuum gate when the gun is in use, is lowered from the glass tube and down through the gate valve, which is then closed, isolating the gun. The gun itself is rigidly attached to the flange which forms a base for the levelers. This is done via an O-ring seal between the flange and the glass encasement for the electron gun.

The copper cup is electrically connected to the aluminum cylinder via stainless steel springs as shown in Figure 4. These springs are soldered to the cup and press against the aluminized layer inside the glass tube. Both the cup and aluminum layer are maintained at 15 kilovolts with respect to ground by an oil insulated D.C. power supply, fed by shielded cable and a high-voltage pyrex window which is shown in

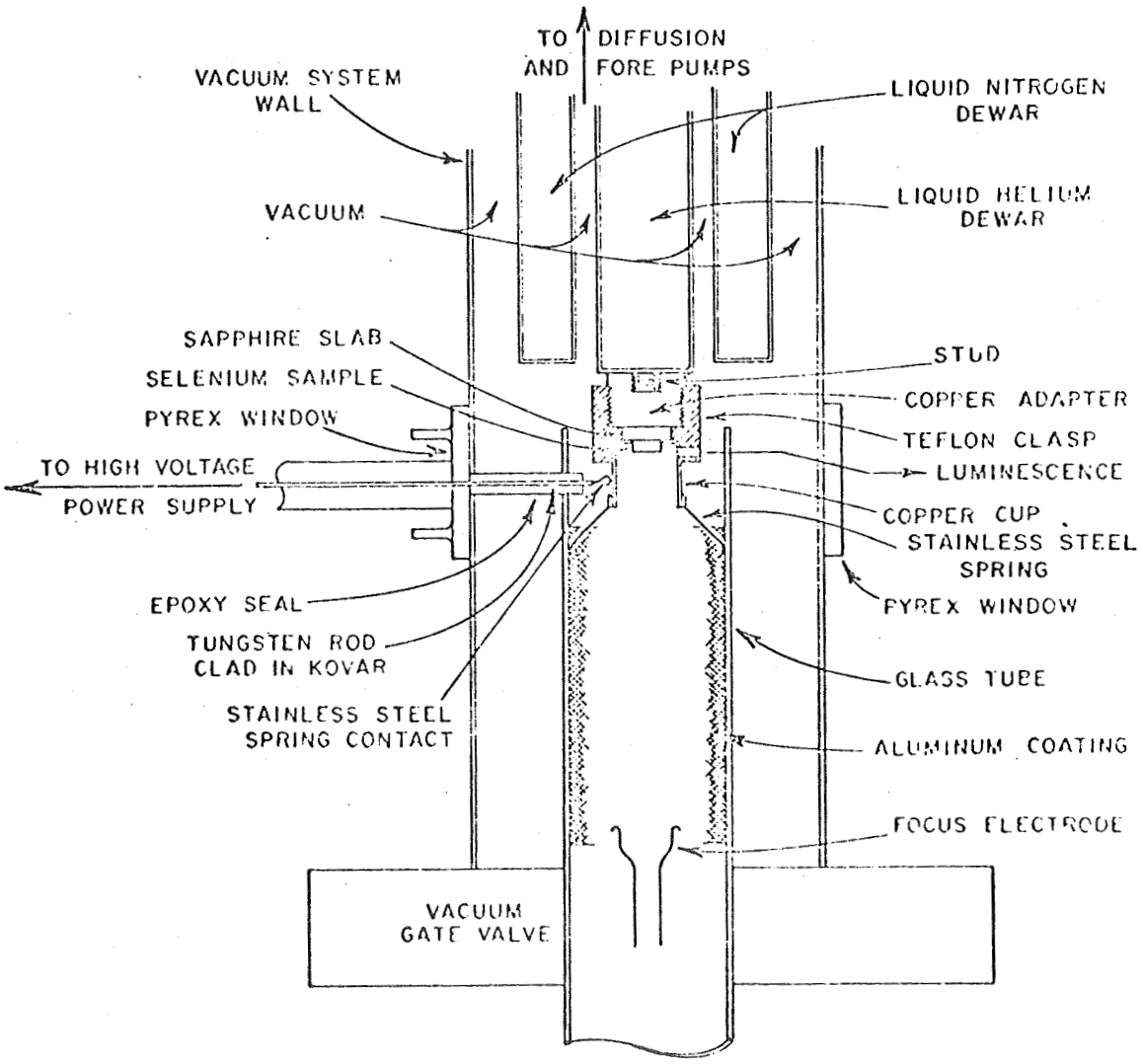

Figure 4. Details of Work Area of Apparatus.

Figure 5. The tungsten rod is clad with kovar to form a good glass (pyrex) to metal seal. A low vapor pressure epoxy seal surrounds the tungsten rod after it enters the vacuum system. This epoxy seal serves three functions. First, it strengthens the glass-metal seal to prevent damage. Second, it lengthens the arc-over path from the rod to the metal shell of the vacuum system, helping to prevent arcing. Third, it supports the glass tube with the aluminum coating. The epoxy has been shaped to approximate a cylinder co-axial with the rod, and a hole has been drilled in the side of the tube, above the aluminum coating. The epoxy seal fits inside this hole.

The cup and the teflon clasp which surrounds it have small coaxial holes in them to permit observation of luminescence as indicated in Figure 4. The selenium is held in the cup by a thin round metal clip across its surface. Thus, the aluminum coating, the copper cup, and the selenium sample form an anode system with the focused electron beam striking the selenium. The anode cup must be thermally connected to the dewar but electrically isolated from it so that the entire dewar system is not at dangerously high voltages. Thermal contact and electrical isolation is achieved by using a slab of sapphire about 1 cm thick. The anode cup has circumferential tabs so that the teflon supports it in bayonette clip fashion. The cup is gold-plated on the inside to reduce radiative heat loss from the sample.

The copper adapter shown in Figure 4 is a solid cylinder with the bottom polished flat. It is threaded externally and a hole in its top surface is also threaded. The adapter is first threaded into the

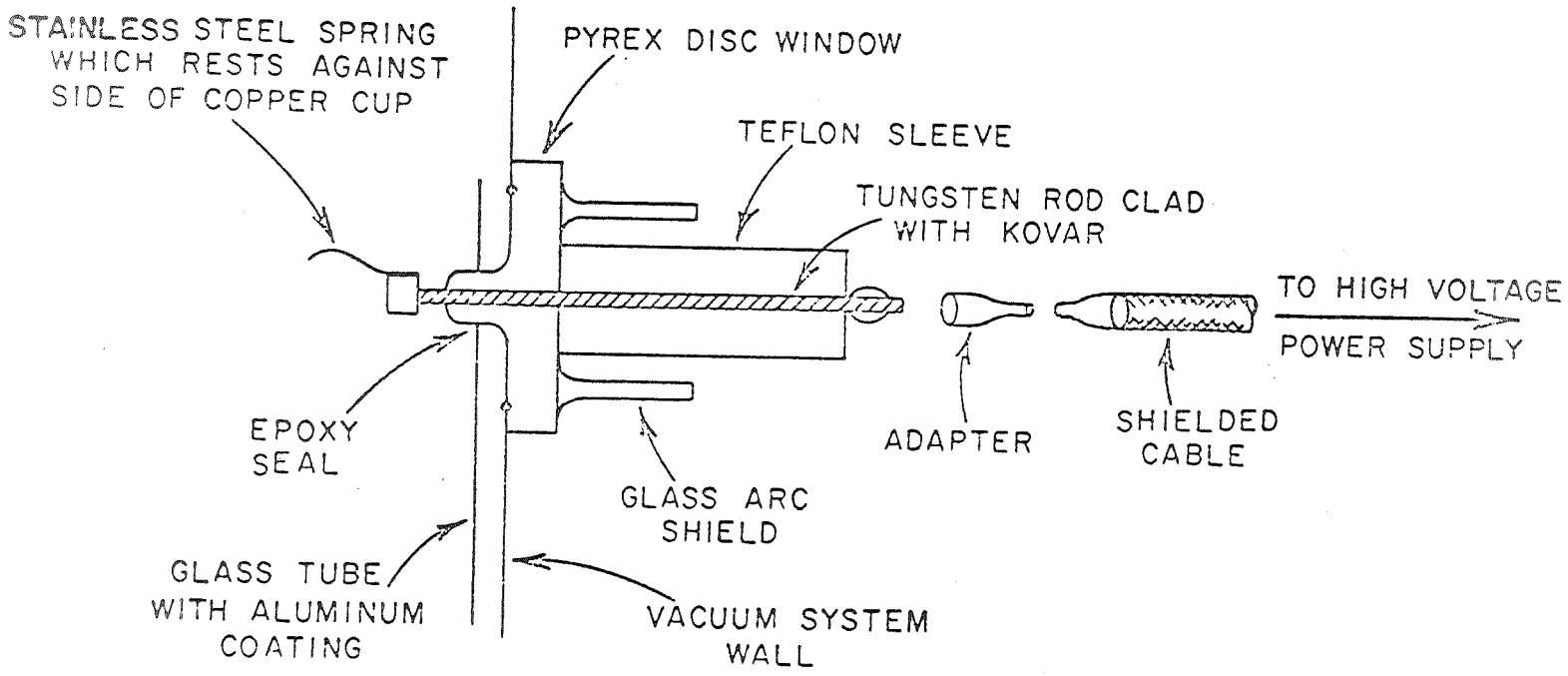

Figure 5. Details of High Voltage Feedthrough.

top of the teflon clasp until the copper cup, the sapphire, and the adapter are in loose contact. Contraction of the clasp at cryogenic temperatures insures a snug fit and a good path for thermal conduction. Finally, the adapter-slab-cup-clasp assembly is threaded onto the stud on the liquid helium dewar.

After the vacuum system is sealed, the fore pump and diffusion pump are sequentially operated, bringing the pressure in the vacuum system down to about 2×10^{-4} torr. The electron gun is still isolated from the rest of the system, and is at a somewhat lower pressure. The liquid nitrogen jacket was heretofore empty, so that no moisture would accumulate on the outer surfaces of the jacket prior to evacuation of the system. The jacket is now filled, reducing the pressure to about 2×10^{-6} torr. The vacuum gate is now opened and the electron gun raised into position. After a short period of pressure stabilization, liquid helium is transferred into the helium dewar, reducing the pressure to about 3×10^{-7} torr. With the control electrode biased to cut off cathode current, the heater of the electron gun is turned on and brought up to specified operating voltage and current.

The electron gun used is of the type used in the 7NP4 projection kinescope, and uses an oxide cathode. It has been found that if the heater is activated before the liquid helium is transferred into the dewar, the heat from the filament causes the pressure to rise to levels at which the cathode begins to deteriorate. The threshold level of deterioration seems to be about 3×10^{-6} torr, except during momentary high voltage arc-overs, which probably don't cause

deterioration even though the pressure may rise to 5×10^{-6} torr or higher. Deterioration of the cathode is evidenced by discoloration, which may be seen after the gun has been replaced.

After the heater temperature and the system pressure have restabilized, the first accelerator voltage supply and the cathode and anode voltage supplies are set as indicated earlier in the chapter and in Figure 2. Upon application of positive pulses to the control electrode, as indicated earlier, pulses of cathode beam current are released. The external micrometer levelers are adjusted for maximum luminescent intensity. The cathode and anode voltages are now separately adjusted for better focus of the electron beam on the target sample, as discussed in Appendix II.

It is believed that cathodoluminescence has been observed in monocrystalline hexagonal selenium in one instance to date. It was not possible to confirm this observation by spectral measurement. Presumably, high spectral intensity in the region of 6820 Å (1.82 eV) would indicate cathodoluminescence conclusively. A glow which appeared red to the human eye was observed, but it disappeared during attempts to intensify the glow by micrometer leveler adjustment. Also, reflection of the heater glow in the round metal clip which holds the sample in the anode cup tends to obscure luminescence.

As an operational test of the experimental apparatus, platelets of CdS were placed in the anode cup instead of the sample of selenium. The cathode voltage was set at about 4 kilovolts, negative

with respect to ground, and the anode at about 16 kilovolts positive. Strong green luminescence was observed to emanate from the CdS.

High voltage arcing-over continues to be somewhat of a problem. It occurs regularly throughout the period of observation, and could possibly frustrate attempts to use conventional, slow spectrometers to measure luminescence.

Much progress has been made however, because arcing-over had frequently tripped circuit breakers before even cursory observations could be made. This difficulty has been lessened by making all possible arc-over paths as long as possible.

It was found desirable to monitor the cathode and anode currents in order to better diagnose certain electrical difficulties which arose during some experiments. A coil of wire was wound on a ferrous torroidal core. Two such coils were constructed. One was slipped over the cathode lead, and the other over a portion of the anode cable near the adapter (shown in Figure 5), where the shielding braid had been trimmed back. The voltages induced in the monitoring coils were proportional to the time rates of change of the pulsed currents and could be viewed on an oscilliscope.

CHAPTER V. CONCLUSION

Cathodoluminescence has been observed in platelets of cadmium sulfide at 4.2°K bombarded by an electron beam with an energy of approximately 20 keV. It is believed that cathodoluminescence has been observed in single crystals of hexagonal selenium at 4.2°K under bombardment by 20 keV electrons. Spectrographic verification of this observation has not yet been possible, but the luminescence appeared to be in the red portion of the spectrum, as is expected from the absorption measurements and photoluminescent studies of others.

Progress in this investigation should yield valuable information regarding the band structure and optical properties of monocrystalline hexagonal selenium, and this effort could possibly be extended to the construction of lasers using selenium and selenium-tellurium alloys as active media.

APPENDIX II

ELECTRON BEAM FOCUSING

A beam of electrons may be focused by an electrostatic lens in a manner similar to the way a beam of light is focused by an optical lens.

Three coaxial cylindrical shells are shown in Figure 6. Consider the beam of electrons propagating along this axis from left to right through cylinder No. 1. Assume that the diameters of the three cylinders are equal. Let cylinder No. 1 be at an electrostatic potential, V_1, and let cylinders No. 2 and No. 3 be at potentials V_2 and V_3, respectively. Assume that V_1, V_2, and V_3 are negative with respect to ground, although the discussion is valid even if they aren't. Furthermore, assume that $V_1<V_2<V_3$. The region within one cylinder radius of the common axis and in the vicinity of the interface between one cylinder and another is a type of electrostatic lens known as a "bipotential lens". Thus, the center of one electrostatic lens lies in the plane A-A', and the center of another in the plane C-C'.

If the diameter of the beam of electrons as it passes through cylinder No. 1 is small compared to the diameter of the cylinders, then when the beam propagates into the region to the right of the plane A-A', it will be focused at the point B. To the right of the point B, the beam diverges. The exact distance of the point B from the plane A-A' is determined by the ratio V_2/V_1. If the diameter

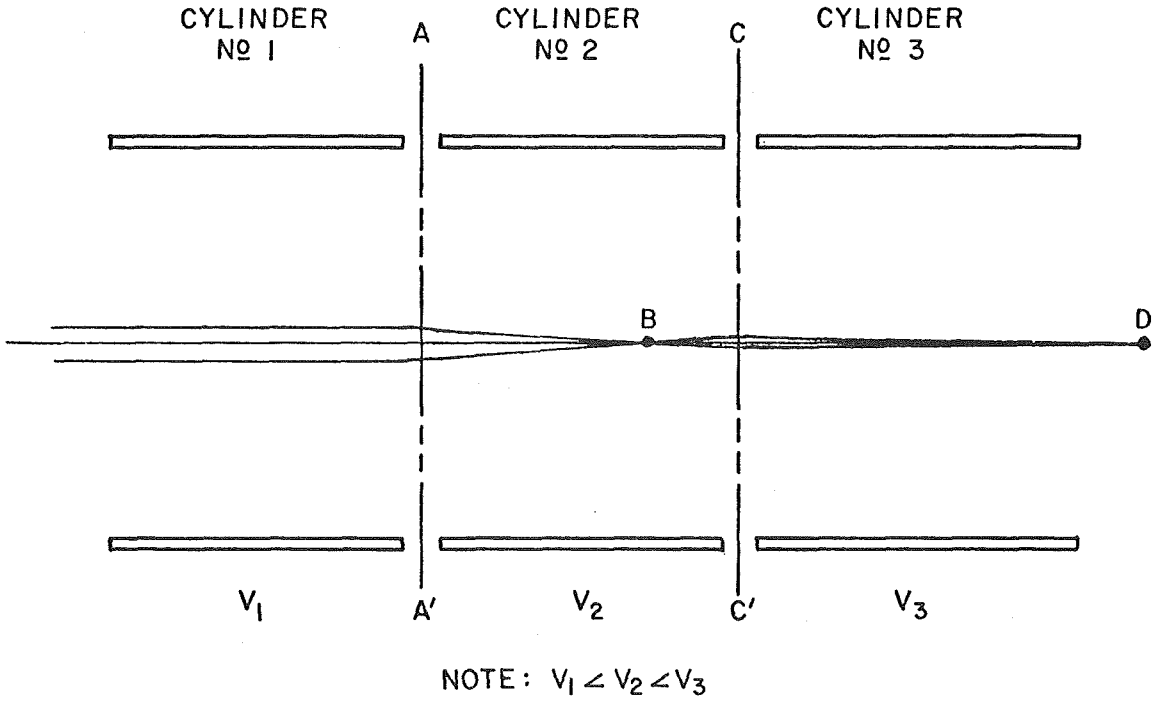

Figure 6. Electrostatic Focusing of an Electron Beam.

of the divergent beam at the plane C-C' is small compared to the diameter of the cylinders No. 2 and No. 3, the beam will be focused at the point D. The exact distance of the point D from the plane C-C' is determined by the ratio V_3/V_2.

The focusing arrangement used in the experimentation described above consists of a cathode lens and two bipotential lenses. The cathode lens consists of the cathode, the control electrode, and the front of the first accelerator. It delivers an essentially parallel beam of electrons to the first bipotential lens, consisting of the back end of the first accelerator and the narrow front end of the focus electrode. The beam is then focused by this lens and is subsequently refocused onto the sample by the second bipotential lens formed by the wide mouthpiece of the focus electrode and the cylindrical aluminum coating.

The focal length of the first bipotential lens may be found from a chart prepared by Zworykin, et.al.[16] which plots the focal distances of equidiameter coaxial cylindrical lenses as a function of the ratio of the potentials on the two cylinders. If the cathode potential is taken as the reference, the first accelerator is at + 500 volts, while the focus electrode is at + 5500 volts. Both of these cylindrical electrodes have a diameter of 10 mm. From the chart cited above, the focal length of the first lens is about 1.1 diameters, or 11 mm, measured from the interface between the two cylinders.

The second bipotential lens consists of the focus electrode mouthpiece, which is 20 mm in diameter, and the aluminum cylinder coating, which is 48 mm in diameter. Thus, the diameter ratio is 2.4, and the voltage ratio is 4:1 because the aluminum cylinder is at 20 kilovolts, and the focus electrode is at 5 kilovolts, both positive with respect to the cathode. Another chart prepared by Zworykin, et.al.[16] indicates that the focal length is 4.75 times the diameter of the focus electrode, or 95 mm measured from the interface between the two cylinders.

Assuming an essentially parallel beam entering bipotential lens No. 1, the image of that lens forms the object of bipotential lens No. 2. Since the focus electrode is 96 mm long and the first image is 11 mm beyond lens No. 1, the object distance of lens No. 2 is 85 mm. Using the thin lens formula

$$\frac{1}{f} = \frac{1}{s_i} + \frac{1}{s_o}$$

where f is the focal length of the lens, and s_i and s_o are the distances of the image and the object from the lens, it is found that the electron beam is focused 807 mm from the end of the focus electrode mouthpiece.

REFERENCES

(1) Hurwitz, C. E., Appl. Phys. Letters, 9, 420 (1966).

(2) Hurwitz, C. E., and Keyes, R. J., Appl. Phys. Letters, 5, 139 (1964).

(3) Benoit à la Guillaume, C., and Debever, J. M., Solid State Comm., 2, 145 (1964).

(4) Benoit à la Guillaume, C., and Debever, J. M., Solid State Comm., 3, 19 (1965).

(5) Zetsche, H., and Fischer, R., J. Phys. Chem. Solids, 30, 1425 (1969).

(6) Queisser, H. J., and Stuke, J., Sol. State Comm., 5, 75 (1967).

(7) Gobrecht, H., and Tausend, A., Z. f. Phys., 161, 205 (1961).

(8) Treusch, J., and Sandrock, R., Phys. Stat. Sol., 16, 487 (1966).

(9) Olechna, D. J., and Knox, R. S., Phys. Rev., 140, A986 (1965).

(10) Stuke, J., and Keller, H., Phys. Stat. Sol., 7, 189 (1969).

(11) Tutihasi, S., and Chen, I., Sol. St. Comm., 5, 255 (1967).

(12) Roberts, G. G., et.al., Phys. Rev., 166, 637 (1968).

(13) Sproull, R. L., Modern Physics, John Wiley & Sons, Inc., pp. 364-365 (1966).

(14) Klein, C. A., Physics of Quantum Electronics, McGraw-Hill, pp. 424-434 (1966).

(15) Anderson, W. W., Applied Optics, 5, 167 (1966).

(16) Zworykin, V. K., et.al., Electron Optics and the Electron Microscope, John Wiely & Sons, Inc., pp. 450-452 (1945).